frontiers in Earth Science

ORIGINAL RESEARCH
published: 26 April 2021
doi: 10.3389/feart.2021.641654

Trace Element Signatures in Pyrite and Marcasite From Shallow Marine Island Arc-Related Hydrothermal Vents, Calypso Vents, New Zealand, and Paleochori Bay, Greece

Mark Nestmeyer[1], Manuel Keith[1], Karsten M. Haase[1], Reiner Klemd[1], Panagiotis Voudouris[2], Ulrich Schwarz-Schampera[3], Harald Strauss[4], Marianna Kati[2] and Andreas Magganas[2]*

[1]GeoZentrum Nordbayern, Friedrich-Alexander Universität (FAU) Erlangen-Nürnberg, Erlangen, Germany, [2]National and Kapodistrian University of Athens, Faculty of Geology and Geoenvironment, University Campus, Athens, Greece, [3]Bundesanstalt für Geowissenschaften und Rohstoffe, Hannover, Germany, [4]Institut für Geologie und Paläontologie, Universität Münster, Münster, Germany

OPEN ACCESS

Edited by:
Jon Hawkings, Florida State University, United States

Reviewed by:
Ziming Yang, Oakland University, United States
Andrew Martin, Memorial University of Newfoundland, Canada

***Correspondence:**
Mark Nestmeyer
marknestmeyer@outlook.de

Specialty section:
This article was submitted to Geochemistry, a section of the journal Frontiers in Earth Science

Received: *14 December 2020*
Accepted: *17 February 2021*
Published: *26 April 2021*

Citation:
Nestmeyer M, Keith M, Haase KM, Klemd R, Voudouris P, Schwarz-Schampera U, Strauss H, Kati M and Magganas A (2021) Trace Element Signatures in Pyrite and Marcasite From Shallow Marine Island Arc-Related Hydrothermal Vents, Calypso Vents, New Zealand, and Paleochori Bay, Greece. Front. Earth Sci. 9:641654. doi: 10.3389/feart.2021.641654

Fluid conditions of shallow marine hydrothermal vent sites (<200 mbsl) in island arcs resemble those of subaerial epithermal systems. This leads to a distinct mineralization-style compared to deeper arc/back-arc (>200 mbsl) and mid-ocean ridge-related environments (>2000 mbsl). At Calypso Vents in the Bay of Plenty and Paleochori Bay at the coast of Milos Island, fluids with temperatures <200°C are emitted through volcaniclastic sediments in water depths <200 mbsl. The hydrothermal mineralization from these fluids is dominated by pyrite and marcasite showing diverse textures, including colloform alternations, semi-massive occurrences surrounding detrital grains, vein-type pyrite, and disseminated fine-grained assemblages. Pyrite and marcasite from Calypso SE show elevated concentrations of volatile elements (e.g., As, Sb, Tl, Hg) implying a vapor-rich fluid phase. By contrast, elements like Zn, Ag, and Pb are enriched in hydrothermal pyrite and marcasite from Calypso SW, indicating a high-Cl liquid-dominated fluid discharge. Hence, vapor-liquid element fractionation induced by fluid boiling is preserved in the seafloor mineralization at Calypso Vents. Hydrothermal mineralization at very shallow vent sites (<10 mbsl), like Paleochori Bay, are affected by wave action causing a seasonal migration of the seawater-fluid interface in the sediment cover. The $\delta^{34}S$ composition of native S crusts and crystalline S (0.7–6.7‰) is indicative for host rock leaching and thermochemical reduction of seawater sulphate. By contrast, the highly negative $\delta^{34}S$ signature of native S globules in sediments (–7.6 to –9.1‰) is related to microbial sulphate reduction or a subordinate magmatic fluid influx. Alunite-jarosite alteration (Paleochori Bay) and a mineral assemblage consisting of orpiment, realgar, and native S (Calypso Vents) may also suggest a contribution by an oxidised (sulphate-rich) low pH fluid of potential magmatic origin. However, fluid boiling is pervasive at Calypso Vents and Paleochori Bay,

Abbreviations: brt, barite; ccp, chalcopyrite; gn, galena; mt, magnetite; mrc, marcasite; orp, orpiment; py, pyrite; sph, sphalerite; stbn, stibnite, mbsl = metres below sealevel.

and the condensation of vapor-rich fluids in a steam-heated environment may produce a similar alteration and mineralization assemblage without a significant magmatic fluid influx, as known from some subaerial epithermal systems.

Keywords: pyrite trace elements, LA-ICP-MS mapping, Shallow marine hydrothermal vents, island arcs, fluid boiling, Sulfur isotopes, Submarine epithermal analogue

INTRODUCTION

Submarine hydrothermal systems and associated sulphide occurrences are known from a wide range of tectonic settings including mid-ocean ridges, back-arc basins and island arc volcanoes (Fouquet et al., 1993; Hannington et al., 2005; de Ronde et al., 2011; German et al., 2016; Hannington et al., 2017). Magma bodies beneath hydrothermal systems represent the heat sources that drive the circulation of seawater-derived fluids through the oceanic crust, causing chemical exchange and heat transfer between the lithosphere and the oceans (Scott et al., 1974; Von Damm, 1995; Hannington et al., 2005; Tivey, 2007; Stucker et al., 2017; Kleint et al., 2019). Physico-chemical fluid parameters like temperature, pH, redox and the availability of complex forming-ligands (e.g., HS^-, Cl^-, OH^-), together with water depth and host rock composition control the mineralogy and chemistry of seafloor sulphide precipitates (Keith et al., 2014; Seward et al., 2014; Wohlgemuth-Ueberwasser et al., 2015; Keith et al., 2016a; Nozaki et al., 2016; Evans et al., 2020). Island arc and young back-arc hydrothermal systems occur at <2000 m water depth and are typically associated with felsic host rocks enriched in As, Sb, Pb and Tl compared to hydrothermal vents in mature back-arcs and along mid-ocean ridges that are mainly hosted by mafic (to ultramafic) rocks enriched in Co, Ni and Cu at >2000 m water depth (Binns and Scott, 1993; Fouquet et al., 2010; Jenner et al., 2010; Keith et al., 2017; Patten et al., 2017). Submarine vent fields that occur at shallow water depths <200 m are a notable sub-group of island arc-related hydrothermal systems (Prol-Ledesma et al., 2002; Monecke et al., 2014), since they are usually hosted by thick layers of volcaniclastic sediments, which affects the precipitation conditions due to higher degrees of sub-seafloor fluid-seawater mixing enhancing the metal deposition (Pichler et al., 1999; Prol-Ledesma et al., 2002; Valsami-Jones et al., 2005; Price et al., 2013).

Subduction zone magmas commonly reach volatile saturation during their evolution, leading to a release of volatiles that may contribute significant amounts of metals and metalloids with a volatile affinity (e.g., Cu, Au, As, Sb, Tl, Se, Te) to an overlying hydrothermal system (Yang and Scott, 1996; de Ronde et al., 2011; Seewald et al., 2015; Keith et al., 2018b; Patten et al., 2019; de Ronde et al., 2019; Martin et al., 2020). Similar volatile-rich fluids can be produced by boiling, which is a common process in shallow marine (<1500 mbsl) island arc-related hydrothermal systems (Stoffers et al., 2006; Monecke et al., 2014; Diehl et al., 2020). Physical separation of boiling fluids into a high-density alkaline saline liquid and a low-density acidic vapor, rich in volatile species (CO_2, H_2S, H_2, SO_2), is particularly common at low pressure conditions (Drummond and Ohmoto, 1985). Metals and metalloids either partition into the vapor (e.g., As, Sb, Te, Tl, Hg) and liquid phase (e.g., Fe, Co, Ni, Zn, Pb), or alternatively precipitate during fluid boiling (e.g., Au; Pokrovski et al., 2013; Brugger et al., 2016; Gartman et al., 2018; Román et al., 2019; Keith et al., 2020). Boiling and vapor-dominated venting (gas bubbling) were observed at several shallow marine and lacustrine hydrothermal vent fields, such as Lake Taupo, New Zealand (de Ronde et al., 2002); the west coast of Mexico (Prol-Ledesma et al., 2002; Canet et al., 2005); Lihir Island, Papua New Guinea (Pichler et al., 1999); Paleochori Bay, Milos, Greece (Valsami-Jones et al., 2005), and offshore Kueishantao islet, Taiwan (Chen et al., 2005; Yu et al., 2019). Magmatic volatile influx and vapor-dominated fluid venting lead to a mineralization- (e.g. native S) and alteration-style (advanced argillic) in shallow marine island arc-related settings that is partly comparable to subaerial epithermal systems reflecting volatile-rich and acidic fluid conditions (Naden et al., 2005; Alfieris et al., 2013; Yeats et al., 2014; Wu et al., 2016; Seewald et al., 2019; Yu et al., 2019).

Pyrite is a common constituent in hydrothermal precipitates and incorporates a wide range of trace elements under highly variable fluid conditions (e.g., temperature, pH, redox). Hence, trace element contents and stable isotope variations (e.g. $\delta^{34}S$) in pyrite allow us to monitor changes in fluid composition related to processes like fluid boiling and magmatic volatile influx (Wohlgemuth-Ueberwasser et al., 2015; Keith et al., 2016a; Keith et al., 2016b; Maslennikov et al., 2017; Martin et al., 2019; Román et al., 2019; Keith et al., 2020; Martin et al., 2020). However, the trace element composition of hydrothermal pyrite in shallow marine hydrothermal systems (<200 mbsl) has not been investigated to date, and hence little is known about the enrichment processes of trace metals and metalloids in these environments (Valsami-Jones et al., 2005; Wu et al., 2016; Houghton et al., 2019). In a recent study, the mineralogical and major (and minor) element composition of hydrothermal pyrite and marcasite from Paleochori Bay (Milos, Greece) has been described and related to the venting of high-Cl liquid- and low-Cl vapor-dominated fluids (Voudouris et al., 2021). We significantly extend this approach by a micro-analytical trace element study combined with S isotope analyses on samples from Paleochori Bay and Calypso Vents (Bay of Plenty, New Zealand). We propose a hydrothermal model, in which fluid boiling and seawater mixing are key processes for trace metal and metalloid enrichment and fractionation in shallow marine hydrothermal systems, leading to a mineralization-style that is comparable to some subaerial epithermal systems.

GEOLOGICAL SETTING AND SAMPLE LOCALITIES

Calypso Vents

The Calypso Vents are located within the Bay of Plenty in the Whakatane Graben, the offshore extension of the geothermally

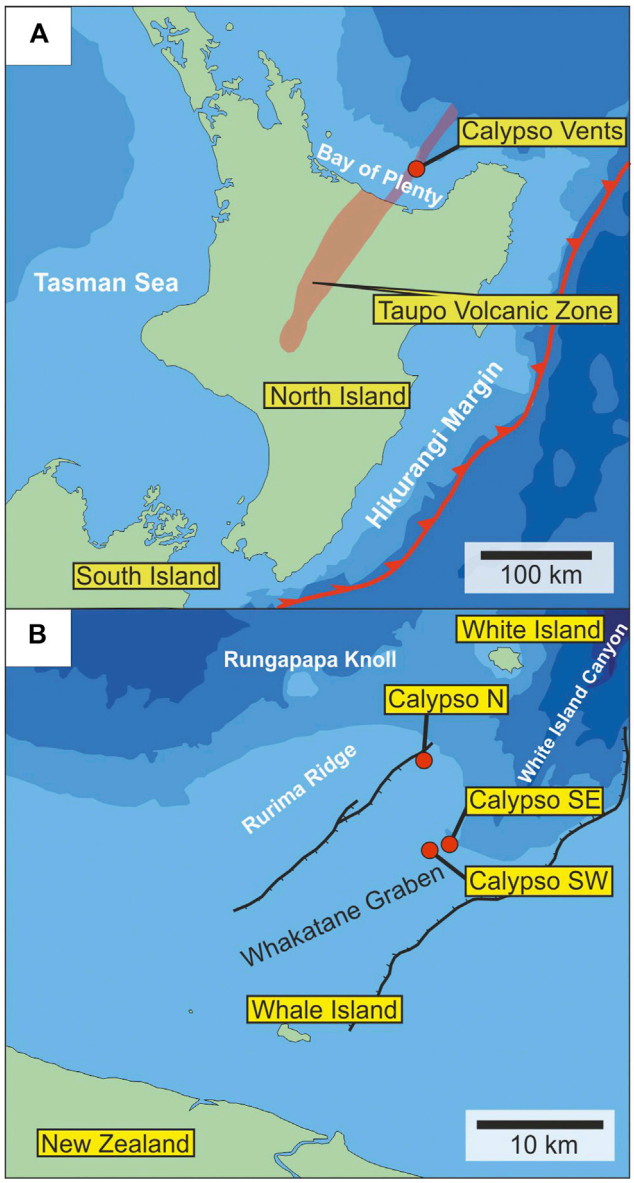

FIGURE 1 | (A) Location of Calypso Vents in the Bay of Plenty on the continental shelf of the northern island of New Zealand (modified after Wilson et al., 1995) **(B)** Location of Calypso N, SE, and SW in the Whakatane Graben between White Island and Whale Island (modified after Wright, 1990).

active Taupo Volcanic Zone, New Zealand (**Figure 1A**; Davey et al., 1995; Wilson et al., 1995). The Pliocene to Quaternary arc volcanism of the Taupo Volcanic Zone results from the subduction of the Pacific Plate underneath the Australian Plate (Davey et al., 1995; Wilson et al., 1995). The Whakatane Graben is located between the volcanoes White Island in the NE and Whale Island in the SW on the continental shelf of New Zealand (**Figure 1B**) hosting a succession of volcaniclastic sediments covering a Mesozoic greywacke basement (Davey et al., 1995; Hocking et al., 2010). Active volcanism occurred on Whale Island during Pleistocene time, whereas White Island is an active volcano hosting a hydrothermal system that may actively form a high-sulfidation Cu-Au mineralization (Hedenquist et al., 1993; Hedenquist and Lowenstern, 1994; Davey et al., 1995). Hydrothermal venting at Calypso is controlled by active late Quaternary normal faulting subparallel to the NW-trending Whakatane Graben (Hocking et al., 2010; Wright 1990). The Calypso hydrothermal system consists of three major vent sites in water depths of 180–190 m: Calypso N, Calypso SW and Calypso SE (**Figure 1B**; Stoffers et al., 1999b). During cruises SO135 in 1998 and SO192/2 in 2007 fluid temperatures between 180 and 200°C were detected at the hydrothermal vents (**Table 1**). Fluid data suggests that CO_2 and minor H_2S are the primary gas species in the hydrothermal fluids (Stoffers et al., 1999a; b; Schwarz-Schampera et al., 2009). In addition to gas bubbling, diffuse discharge of shimmering water has been observed indicating sub-seafloor fluid-seawater mixing (Schwarz-Schampera et al., 2007; Hocking et al., 2010). The main difference between the northern and southern (SE and SW) vent fields is the occurrence of anhydrite and diffuse venting in the north compared to a focused fluid discharge associated with As- and Hg-mineralization and hydrocarbons in the south (Stoffers et al., 1999b).

Paleochori Bay

Paleochori Bay is located in the southeastern coast of Milos Island, Greece, which is part of the active Hellenic island arc forming due to the subduction of the African Plate beneath the Aegean microplate (Voudouris et al., 2019). The forearc region consists of 1) the Cretan forearc basin, 2) a backstop region including the Peloponnese peninsula to the west (mainland Greece), Crete to the south and Rhodes to the east, as well as 3) an accretionary complex, the Mediterranean ridge, located between Crete and the Hellenic Trench (**Figure 2A**; Kopf et al., 2003; Varnavas and Cronan 2005; Price et al., 2013). Milos Island hosts several epithermal deposits associated with geothermal activity (Kilias et al., 2001; Naden et al., 2005; Smith et al., 2018). Shallow submarine hydrothermal venting is concentrated along the southern coastline, where Paleochori Bay is located with its intense hydrothermal activity and As-rich mineralization (Price et al., 2013; Voudouris et al., 2021). Hydrothermal venting is structurally controlled by an active rift, which extends offshore from the subaerial Fyriplaka Volcano (**Figure 2B**; Fytikas et al., 1986; Varnavas and Cronan 2005; Price et al., 2013). Hydrothermal venting occurs in an area of ~35 km^2 and up to 300 m water depth with fluid temperatures reaching 150°C (Yücel et al., 2013). Different types of fluids were described, including low Cl vapor-rich fluids with a focused discharge through volcaniclastic sediments, brine-rich seeps, and low-pH fluids discharging through rock fissures (**Table 1**). Intense discharge also raises sandy/pebbly plumes of volcaniclastic sediments that are cemented by pyrite and marcasite to sulphide mounds, which are associated with gas bubbles and the occasional discharge of saline liquids (Valsami-Jones et al., 2005; Voudouris et al., 2021).

METHODS

Sample Collection, Preparation and Processing

The investigated samples from Calypso Vents were recovered by dredge operations during cruise SO135 from the Calypso N (n =

TABLE 1 | Overview of fluid parameters from Calypso Vents and Paleochori Bay.

Vent field	pH	T [°C]	Depth [mbsl]	References
Calypso N	n/a	201	182	Botz et al. (2002)
Calypso SE	n/a	181	191	Botz et al. (2002)
Paleochori bay	2.08–7.7	4.1–115	0–10	Valsami-Jones et al. (2005)

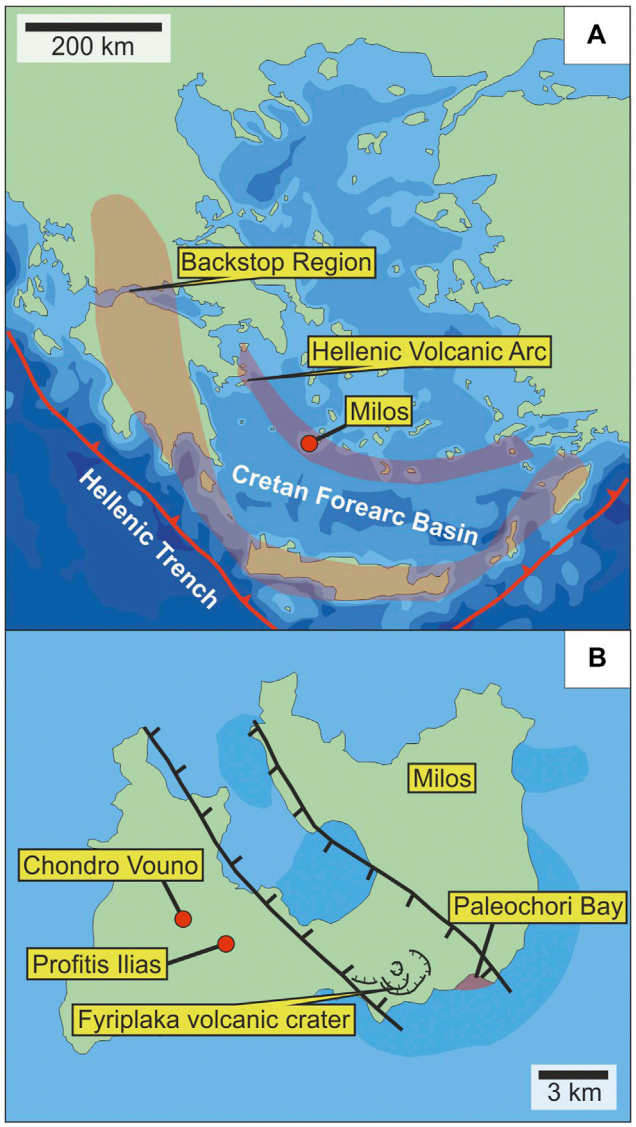

FIGURE 2 | (A) Location of Milos Island in the active Hellenic Volcanic Arc (modified after Kopf et al., 2003; Houghton et al., 2019) **(B)** Milos Island with the neo-tectonic graben structure hosting the hydrothermal vent site of Paleochori Bay. Dark areas indicate fields of hydrothermal activity (modified after Fytikas et al., 1986; Kilias et al., 2001; Houghton et al., 2019).

5), Calypso SE ($n = 3$) and Calypso SW ($n = 6$) vent sites. Samples from Paleochori Bay were recovered by scuba diving from sulphide mounds in the direct vicinity of vent sites with a focused fluid discharge ($n = 4$) at <10 m water depth. Samples of hydrothermal vent fluids were not recovered at Calypso Vents and Paleochori Bay. Polished thin and thick sections ($n = 17$) were prepared from these samples for the following micro-analytical studies (cf. *Micro-Analytical Techniques*) and a fraction of the whole rock specimen was crushed and milled for x-ray diffraction analysis (cf. *X-Ray Diffraction (XRD)*).

X-Ray Diffraction (XRD)

Whole rock samples ($n = 9$) from Calypso Vents (SO135-110DR, -112DR, -112DR2, -112DR3, -113DR7, -118DR5, -116DR3, -118DR2 and -116DR1; **Table 2**) were crushed, milled and mixed with isopropanol. The amalgamation was milled for another 10 min using a McCrone micro mill. The outcome material was subsequently centrifugalised for 10 min and dried at 60 °C for at least 24 h. Subsequent XRD analysis of the homogenous whole rock powders ($n = 9$) was conducted from 2° to 75° 2θ diffraction angle using a Siemens D5000 XRD equipped with a graphite monochromator with Cu Kα radiation at the GeoZentrum Nordbayern. Radiation was set to 40 kV and 35 mA. Samples were analysed for a second time after glycol saturation to improve the clay mineral detection. The XRD patterns were processed by Rietveld refinement using the Profex and BGMN software. Phases that occur in amounts <1 wt% could not be detected by XRD.

Micro-Analytical Techniques

The polished thin and thick sections from Calypso ($n = 13$) and Paleochori Bay ($n = 4$) were examined by optical microscopy and coated with carbon prior to the micro-analytical study. Unknown mineral phases were identified by energy-dispersive spectrometry (EDS) using a TESCAN Vega\\XMU scanning electron microscope at the GeoZentrum Nordbayern. An acceleration voltage of 20 kV and a probe current of 8–11 nA were applied for EDS analysis. Cobalt was used for beam optimization.

The major and minor element composition of pyrite and marcasite was obtained by electron microprobe analysis using a JEOL JXA-8200 Superprobe at the GeoZentrum Nordbayern ($n = 267$). Wavelength-dispersive analyses were conducted with a focused beam, an acceleration voltage of 20 kV and a beam current of 20 nA. Count times were set to 20 and 10 s for the peak and background measurements, respectively. The following reference materials were used for the standardization: $CuFeS_2$ (for S, Fe, Cu) and InAs (for As), InSb (for Sb), Co (for Co), Ni (for Ni), ZnS (for Zn), PbS (for Pb). Analyses with a total mass <98 wt %, >101 wt% or with an error >3 at% with respect to the stoichiometric composition were discarded. The Co, Ni, Cu, Zn, Sb and Pb concentrations in pyrite and marcasite determined by electron microprobe were not used for further interpretation, because concentrations were usually <0.1 wt%

TABLE 2 | List of sample localities and mineralogical composition of the hydrothermal mineralization at Calypso Vents and Paleochori Bay.

Vent field	Sample no	Latitude	Longitude	Hydrothermal mineralization	Depth [mbsl]
Calypso SE	SO-135–110DR	–37°41.31′	177°07.34′	opal, py, mrc, native S, Zn-Hg-sulphide	189–192
Calypso SW	SO-135–112DR	–37°41.62′	177°06.06′	brt, sph, gn, orp, stbn, py, ccp, Ag-sulphide	184–185
Calypso SW	SO-135–112DR2	–37°41.62′	177°06.06′	brt, sph, gn, orp, stbn, py	184–185
Calypso SW	SO-135–112DR3	–37°41.62′	177°06.06′	py, cal	184–185
Calypso SW-SE	SO-135–113DR7	–37°41.74′	177°06.98′	mrc, py	187–188
Calypso N	SO-135–118DR5	–37°36.83′	177°06.08′	py, ill? smc? hm	161–166
Calypso N	SO-135–116DR3	–37°36.83′	177°05.63′	mrc	161–166
Calypso N	SO-135–118DR2	–37°36.83′	177°06.08′	mrc	163–170
Calypso N	SO-135–116DR1	–37°36.83′	177°05.63′	py	163–170
Paleochori bay	Mil-4–3	36°40.440’	24°30.949′	py, mrc	<10
Paleochori bay	Mil-3	36°40.440′	24°30.949′	mrc, py, sulphosalts	<10
Paleochori bay	Mil-4	36°40.440′	24°30.949′	mrc, py, sulphosalts	<10
Paleochori bay	Mil-3–302	36°40.440′	24°30.949′	mrc, py, sulphosalts	<10

Abbreviations: brt, barite; cal, calcite; ccp, chalcopyrite; gn, galena; hm, hematite; ill, illite; smc, smectite; mrc, marcasite; orp, orpiment; py, pyrite; sph, sphalerite; stbn, stibnite; mbsl, metres below sealevel.

(**Supplementary Table S1**), which is close to or below the detection limit but well within the capability range of LA-ICP-MS.

The trace element composition of pyrite and marcasite was determined by LA-ICP-MS using a Teledyne Analyte Excite 193 nm laser coupled with an Agilent 7500c ICP-MS system at the GeoZentrum Nordbayern (n = 157). The plasma power of the ICP-MS system was set to 1300 W. Helium (0.9 L/min) and Ar (0.94 L/min) were used as carrier gases. In addition, Ar was used as plasma (14.9 L/min) and auxiliary gas (0.9 L/min). A single spot ablation pattern with a frequency of 15 or 20 Hz and a fluence of 4.04 J/cm^2 was used. A beam diameter of 10–25 µm was applied according to pyrite and marcasite crystal size. Total analysis time was set to 40 s including 20 s of pre-ablation blank analysis. The Po724 B2 SRM (Sulphide Memorial University Newfoundland) (Au) and MASS-1 (USGS) (Co, Ni, Cu, Zn, Ga, Ge, As, Se, Mo, Ag, Cd, In, Sb, Te, Hg, Tl, Pb and Bi) reference materials were used for the external calibration. A stoichiometric value of 53 wt% S was used for the internal standardisation of pyrite and marcasite. Trace element and minimum detection limits were processed by GLITTER (**Supplementary Table S2**; van Achterbergh et al., 2000). Data quality was monitored by the repeated analysis of the sulphide standards yielding a relative standard deviation (RSD) of <10% for Ga, As, Mo, Cd, In, Sb, Pb and Bi; <15% for Cu, Zn, Ge, Se, Ag, Te, Au, Hg and Tl; <17% for Co and Ni. Quantitative spot analysis was combined with qualitative LA-ICP-MS mapping to visualise trace element distribution patterns in individual crystals or fine-grained pyrite-marcasite assemblages. A square-shaped beam of 5 µm at a scan speed of 3 µm/s and a repetition rate 15 Hz was applied for the mapping. All other operating conditions were identical to the spot analysis. The qualitative trace element maps were processed by the iolite software package developed at the University of Melbourne (https://iolite-software.com).

Geochemical data from natural systems rarely show a normal distribution, and hence the geometric mean and geometric standard deviation (GSD) were used to measure central tendency and dispersion, respectively (**Table 3**; Reimann and Filzmoser, 2000).

Sulfur Isotope Analysis

Sulfur isotope measurements were performed on native S separates (n = 5) from Calypso Vents (SO135-88DR, -110DR02, -103DR2, -98DR and -103DR1) without further chemical treatment (**Supplementary Table S3**). About 48–55 µg of S and 300–500 µg of V_2O_5 were placed into tin capsules. Subsequent isotope analysis was performed using a Carlo Erba elemental analyser coupled with a ThermoFinnigan Delta Plus isotope ratio mass spectrometer (EA-IRMS) at the Westfälische Wilhelms-Universität Münster. Reproducibility as determined through replicate analyses of reference materials was better than ±0.2‰ (1σ) and precision of duplicate measurements was <0.7‰. Values are presented in per mille difference relative to the Vienna-Canyon-Diablo Troilite (V-CDT) standard.

RESULTS

Hydrothermal Mineralogy

Pyrite and marcasite are the dominant sulphides in most samples from Calypso Vents (**Table 2**), where they are commonly disseminated in the host lithologies as anhedral to subhedral crystals. Locally framboids, veins or coatings of pyrite and/or marcasite around silicate grains or Fe-Ti-oxides were observed (**Figure 3A**). The hydrothermal mineralization at Calypso SE is characterised by massive opaline silica and a pyrite (-marcasite) vein-related mineralization that occurs between ash layers (**Table 2**; **Figure 3B**). Back-scattered electron imaging exhibits concentric/growth zoning in vein-type pyrite, in which the light grey spherical zones contain inclusions of a Zn-Hg sulphide (**Figure 3C**). In addition, a pumiceous tuff sample was recovered between Calypso SE and SW, which hosts macroscopic fragments of charcoal associated with the pyrite and marcasite mineralization (**Supplementary Figure S1B**). By contrast, the samples from Calypso SW are mainly composed of barite with minor chalcopyrite and sphalerite that hosts galena inclusions (**Figure 3D**). Pyrite is locally associated with a Ag-rich sulphide phase, probably an argentite or acanthite polymorph (Ag_2S, **Figure 3E**). Radial orpiment locally surrounds skeletal

TABLE 3 | Compilation of trace element concentrations in pyrite and marcasite from Calypso Vents and Paleochori Bay.

Vent field/Min. Type		Co [ppm]	Cu [ppm]	Zn [ppm]	As [ppm]	Mo [ppm]	Ag [ppm]	Sb [ppm]	Hg [ppm]	Tl [ppm]	Pb [ppm]
Calypso SE	Min	0.24	1.19	209	14,545	22.4	0.03	0.07	2.40	0.66	0.17
py fine-grained	Max	11.5	8.19	321	35,538	40.0	0.07	0.30	85.7	3.11	3.61
n = 8	Geomean	0.61	2.34	272	28,383	30.5	0.05	0.16	15.6	1.59	0.49
	GSD	3.45	2.97	1.15	1.33	1.19	1.46	2.11	3.56	1.74	3.12
Calypso SE	Min	0.11	b.d.l.	32.0	2599	18.6	0.05	0.22	10.6	2.09	0.10
py vein-type	Max	0.14	b.d.l.	284	32,529	47.3	0.05	16.2	2037	554	1.37
n = 10	Geomean	0.12	n/a	76.2	6511	28.9	0.05	1.33	554	215	0.20
	GSD	1.20	n/a	2.09	2.27	1.36	n/a	4.53	4.27	5.19	2.45
Calypso SE	Min	5.34	8.15	278	575	4.81	0.10	1.55	17.9	13.5	7.08
mrc fine-grained	Max	81.3	127	832	4387	59.1	0.57	27.7	246	384	882
n = 9	Geomean	20.6	43.3	464	1334	18.4	0.28	8.05	104	119	117
	GSD	3.04	2.68	1.47	1.85	2.16	1.92	2.50	2.33	3.80	4.07
Calypso SW	Min	0.17	1339	577	307	2.13	1068	305	12.2	52.4	3614
py fine-grained	Max	12.4	5515	22,897	10,650	127	10,680	11,239	366	9190	23,747
n = 18	Geomean	1.28	2527	3269	1903	15.2	3246	1808	63.5	1136	10,315
	GSD	3.81	1.45	3.33	2.73	3.34	2.04	2.92	2.99	4.84	1.64
Calypso SW	Min	0.72	63.95	19.5	15.5	5.83	0.02	0.83	1.45	0.24	1.51
mrc fine-grained	Max	512	388	29,144	353	64.0	0.27	42.3	30.4	7.08	45.8
n = 22	Geomean	34.5	141	82.9	75.1	24.3	0.07	4.03	12.0	2.35	10.2
	GSD	4.20	1.70	5.42	2.08	1.94	2.13	2.43	2.12	2.14	2.77
Calypso N	Min	0.11	1.45	1.88	15.2	0.05	0.03	0.40	0.20	0.01	2.38
py fine-grained	Max	96.7	76.6	338	5665	35.3	1.97	44.6	217	26.7	269
n = 18	Geomean	6.90	15.4	8.78	592	1.95	0.34	9.86	15.9	4.24	35.2
	GSD	6.99	3.07	4.59	5.51	5.09	3.16	2.86	5.02	5.89	3.93
Calypso N	Min	0.10	2.96	16.9	0.40	0.13	0.04	0.20	0.90	0.05	0.30
mrc fine-grained	Max	60.0	95.0	255	534	8.86	2.68	0.36	1.95	0.40	44.0
n = 10	Geomean	1.47	15.4	47.9	4.37	0.71	0.46	0.27	1.42	0.18	1.46
	GSD	9.81	3.42	2.42	12.2	5.33	4.65	1.52	1.43	1.86	4.54
Paleochori bay	Min	0.77	2.19	48.5	272	1.94	0.06	1.02	0.93	5.40	6.64
py colloform	Max	93.5	179	227	4250	10.8	20.3	13.4	3008	107	613
n = 10	Geomean	6.59	8.26	103	1141	4.43	0.30	5.69	6.07	32.2	59.1
	GSD	5.04	3.65	1.83	2.59	1.83	7.60	2.19	15.1	2.58	4.35
Paleochori bay	Min	0.19	0.41	16.5	181	0.70	0.01	1.04	0.58	0.40	0.28
mrc colloform	Max	97.1	13.6	177	11,122	14.8	1.78	64.8	155	75.8	3863
n = 31	Geomean	1.80	3.01	57.6	1051	3.14	0.13	7.76	17.0	9.76	13.1
	GSD	3.99	2.79	1.91	3.00	2.09	3.62	2.71	5.54	4.07	9.12
Paleochori bay	Min	10.7	2.86	53.1	9828	5.53	0.05	170	7.21	4738	280
py semi-massive	Max	58.9	56.4	328	25,732	19.9	0.48	2670	178	8868	3407
n = 7	Geomean	31.2	13.8	124	17,607	10.8	0.23	996	56.5	6482	1402
	GSD	1.76	2.81	2.26	1.43	1.48	2.25	2.60	2.88	1.28	2.41
Paleochori bay	Min	0.51	0.22	80.1	456	6.05	0.03	4.21	0.34	639	3.44
mrc semi-massive	Max	28.7	28.2	3234	12,257	78.5	0.19	754	147	5112	1408
n = 14	Geomean	4.74	2.59	310	1469	16.8	0.05	23.3	1.30	1816	23.9
	GSD	3.02	4.90	2.72	2.51	2.06	2.08	3.48	4.80	1.74	4.47

*The full data set is presented in the **Supplementary Table S2**. Abbreviations: py, pyrite; mrc, marcasite; GSD, Geometric Standard Deviation, b.d.l., below detection limit.*

stibnite in the barite-cemented tuffs of Calypso SW (**Figure 3F**). The host lithologies of Calypso N are more diverse compared to the pumiceous tuffs at Calypso SE and SW. This includes, in addition to variably altered (lapilli) tuffs, reworked rhyolitic and granitic host rock compositions. X-ray diffraction patterns of the lapilli-tuffs revealed that illite or smectite are present (**Table 2**). Pyrite and marcasite are the only sulphides identified at Calypso N, which occur as disseminations in the altered host rocks. Additionally, three types of native S can be distinguished at Calypso Vents, including 1) crystalline S that shows a glassy lustre and infills cavities, 2) S crusts cementing the volcaniclastic sediments and 3) mm-sized sulfur globules that are attached to the sample surface (**Supplementary Figure S1A**).

The hydrothermal mineralization at Paleochori Bay primarily consists of pyrite and marcasite. Most samples show several generations of pyrite and marcasite in alternating colloform bands that are interrupted by layers of amorphous silica (**Figures 3G,H**) and sub-microscopic complex Cu, Zn, Ag, Sb and Pb bearing sulphosalts (cf. *Mineral Chemistry*) that were identified by backscattered electron imaging and EDS (**Figure 3I**). Locally, marcasite is attached to silicate pebbles in the volcaniclastic material and is surrounded by pyrite (**Figures 3J,K**), which has an irregular and more porous texture in this assemblage compared to marcasite (**Figures 3J,K**). Host rock-related magnetite typically shows dissolution textures and coatings of Fe-sulphide (**Figure 3L**).

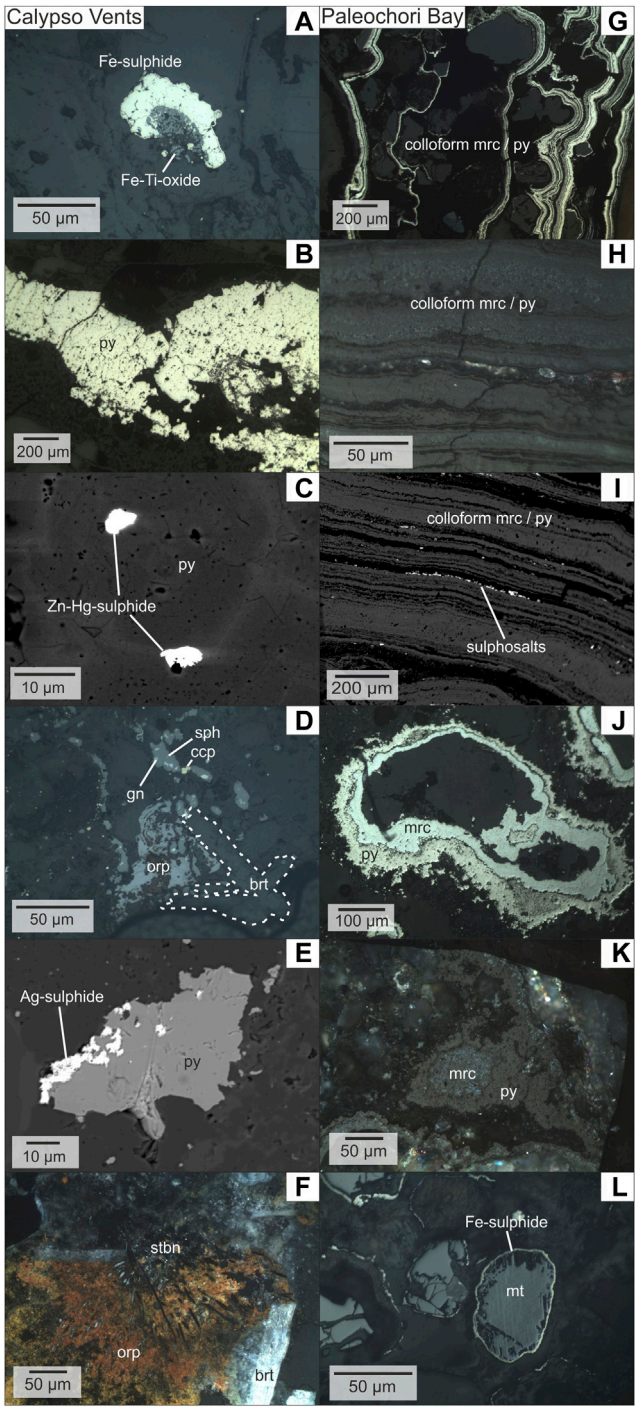

FIGURE 3 | Reflected light photomicrographs and electron images of representative samples from Calypso Vents **(A–F)** and Paleochori Bay **(G–L)**. Calypso Vents **(A)** Fe-sulphide surrounding Fe-Ti-oxide in ash matrix from Calypso SW (112DR3) **(B)** vein-type pyrite from Calypso SE **(C)** inclusions of Hg-Zn sulphide in an As-rich concentric zone in vein-type pyrite from Calypso SE (110DR) **(D)** assemblage of sphalerite, chalcopyrite, galena and orpiment in barite-cemented tuff from Calypso SW (112DR) **(E)** pyrite surrounded by Ag-sulphide (argentite or acanthite) from Calypso SW (112DR) **(F)** skeletal stibnite surrounded by orpiment in barite-cemented tuff from Calypso SW (112DR). Paleochori Bay **(G)** colloform mineralization of

(*Continued*)

Mineral Chemistry

Arsenic concentrations in pyrite and marcasite range from 0.4 ppm to 3.5 wt% (**Table 3**). Vein-type pyrite from Calypso SE shows the highest As contents reaching 3.5 wt%, together with elevated Hg (up to 0.2 wt%) and low Cu, Pb, and Sb (**Table 3**; **Figures 4A–E**). Pyrite in barite-cemented tuffs from Calypso SW displays moderate As (up to 1.1 wt%) and high Pb (up to 2.3 wt %), Sb (up to 1.1 wt%), Zn (up to 2.2 wt%), Ag (up to 1.0 wt%) and Tl (up to 0.9 wt%) contents (**Table 3**; **Figures 4A–E**). Arsenic concentrations in pyrite from Calypso N and Paleochori Bay reach 0.1 and 1.9 wt%, respectively, and show comparable As/Co. ratios and Sb, Ag, Cu, Hg and Pb contents, but distinct Zn and Tl concentrations (**Table 3**; **Figures 4A–E**).

Pyrite and marcasite from Calypso Vents can be distinguished based on their trace element composition. Lead, for example, tends to be enriched in pyrite compared to marcasite from the same vent site (e.g., Calypso N and SW, **Figures 4C,H**). Antimony is enriched in pyrite relative to marcasite at Calypso SW and N, whereas at Calypso SE, pyrite is depleted in Sb compared to marcasite (**Figures 4C,H**). Copper is enriched in pyrite from Calypso SW, but depleted at Calypso SE relative to marcasite from the same vent site. By contrast, pyrite and marcasite from Paleochori Bay generally show a comparable composition (**Figure 4**), and can therefore not be distinguished by their trace element contents. Trace element concentrations also vary with respect to pyrite texture (**Table 3**; **Figure 4E**). For example, As, Sb, Hg (and Tl) are enriched, whereas Co is depleted in vein-type pyrite compared to fine-grained disseminated pyrite from Calypso SE. Semi-massive pyrite and marcasite from Paleochori Bay exhibit higher Tl concentrations than its colloform-textured counterpart (**Figures 4E,J**).

Laser ablation ICP-MS mapping reveals a concentric zoning pattern in vein-type pyrite from Calypso SE, showing a distinct enrichment of Mo, Sb, Hg and Tl in As-rich zones (**Figure 5**), together with an inclusion-related occurrence of Hg (and Zn) (**Figures 3C,5E**; **Supplementary Figure S2**). Trace element maps of colloform pyrite-marcasite from Paleochori Bay display a more complex element distribution, without clear covariations with As (**Figure 6**). Antimony is particularly concentrated in complex Sb, Zn, Cu, Ag and Pb bearing sulphosalts that occur between the pyrite-marcasite layers (**Figure 6**, **Supplementary Figure S3**).

The Shapiro-Wilk-Test show a log-normal distribution for some elements in pyrite and marcasite (Co, Ni, Ge, Cd, Au; $p > 0.05$). A normal distribution was only detected for Se and Te in pyrite ($p = 0.156$ and $p = 0.235$), which is probably related to the small number of analyses ($n < 11$) above the detection limit (**Supplementary Table S4**). Therefore, the non-parametric

FIGURE 3 | alternating pyrite-marcasite in silicate matrix (Mil3-302) **(H)** colloform pyrite-marcasite alternation with amorphous silica layers in crossed polarised light (Mil4) **(I)** back-scattered electron image of colloform pyrite-marcasite with Cu, Zn, Ag, Sb and Pb bearing sulphosalts in amorphous silica layers (Mil3-302) **(J)** pyrite and marcasite surrounding detrital grains in the volcaniclastic sediments (Mil4-3) **(K)** pyrite surrounding marcasite in crossed polarized light (Mil4-3) **(L)** magnetite replacement by Fe-sulphide (Mil4).

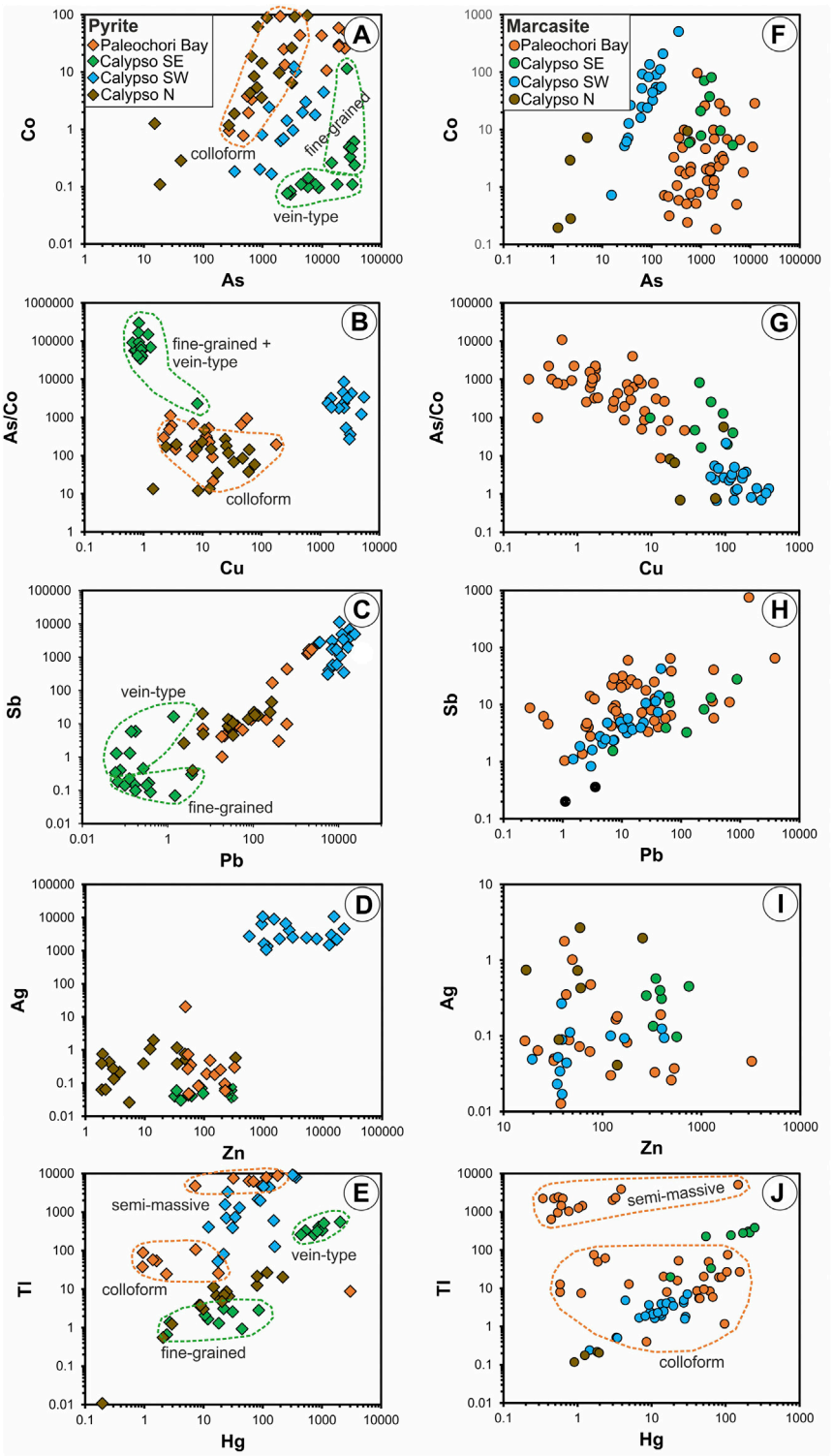

FIGURE 4 | Trace element variation diagrams of pyrite **(A–E)** and marcasite **(F–J)** from Calypso Vents and Paleochori Bay. Note the distinct composition of pyrite and marcasite with respect to mineral texture and the host vent system.

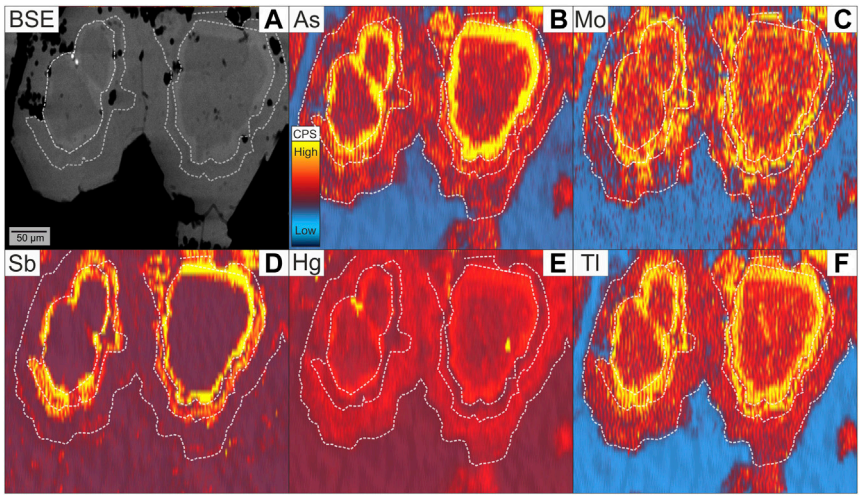

FIGURE 5 | Backscattered electron image **(A)** and trace element maps by LA-ICP-MS **(B–F)** of vein-type pyrite from Calypso SE. Note the Hg-rich inclusions **(E)** in the As-rich zones of pyrite. The white dashed lines represent the crystal margin or separate different zones with distinct trace element composition.

Spearman correlation test was applied. Yielded coefficients (ρ-values) for all bivariate combination and corresponding *p*-values are provided in **Supplementary Table S4**.

Sulfur Isotopes

The $\delta^{34}S$ compositions between the different types of native S (cf. *Hydrothermal Mineralogy*) are highly variable at Calypso Vents, as reflected by negative $\delta^{34}S$ values in S globules (−7.6 to −9.1‰) compared to a positive $\delta^{34}S$ signature in the S crusts (5.7–6.7‰, **Table 4**) and in crystalline S (0.7–3.4‰, **Table 4**). This compositional range in $\delta^{34}S$ is comparable to pyrite and native S from other sediment-covered island arc-related vent sites like Paleochori Bay (−4.4 to −10.8‰; Houghton et al., 2019), Punta Mita (−10.7–4.9‰; Alfonso et al., 2003) and Kueishantao (0.2–2.4‰; Yu et al., 2019). The $\delta^{34}S$ composition of pyrite from the sediment-covered Palinuro volcanic complex (Tyrrhenian Sea) overlaps with Calypso Vents and Paleochori Bay, but extends towards extremely low $\delta^{34}S$ values (−32.8 to −1.1‰; **Table 4**).

DISCUSSION

Precipitation and Alteration Processes

The occurrence of both pyrite and marcasite at Calypso Vents and Paleochori Bay (**Figure 3**) suggests significant fluid temperature and/or pH variations. Marcasite is only stable at pH < 5 and temperatures <240°C (Murowchick and Barnes, 1986), whereas the precipitation of pyrite is not restricted to these fluid conditions, as indicated by a formation at high temperature (up to 400°C) or neutral to alkaline pH (>7) in submarine and subaerial hydrothermal systems (Berkenbosch et al., 2012; Wohlgemuth-Ueberwasser et al., 2015; Keith et al., 2016a, 2020; Meng et al., 2020). Elements like Co and Cu typically precipitate together with their host minerals at fluid temperatures between 300 and 350°C, whereas the solubility of Tl and Pb is not temperature sensitive >220°C (Seyfried and Ding, 1995; Metz and Trefry, 2000). Thus, we expect a Tl and Pb enrichment in marcasite relative to pyrite as a result of the lower formation temperature of the former (<240°C). However, Tl and Pb are not consistently enriched in marcasite compared to pyrite from the same vent site (**Figure 4**), rather excluding a temperature-controlled incorporation. Similarly, colloform pyrite-marcasite, as observed at Paleochori Bay (**Figure 3I**), typically forms by quenching of the discharging fluids with ambient seawater, and therefore represent a low temperature precipitation texture (Berkenbosch et al., 2012; Revan et al., 2014; Grant et al., 2018). However, we do not see a Tl enrichment or Co and Cu depletion in colloform compared to vein-type and semi-massive pyrite-marcasite that commonly form at higher fluid temperatures and more stable precipitation conditions with little fluid seawater-mixing (**Figure 4**; de Ronde et al., 2003; Melekestseva et al., 2014; Wohlgemuth-Ueberwasser et al., 2015; Keith et al., 2016a). This indicates that fluid temperature can likely not explain the trace element variations in pyrite and marcasite and rather suggests that the different crystal structures of cubic pyrite and orthorhombic marcasite may primarily control the trace element distribution at Calypso Vents and Paleochori Bay (cf. *Fluid Boiling and Metal Deposition*). The low fluid temperatures at Calypso Vents (<200°C) and Paleochori Bay (<115 °C; **Table 1**) also suggest a low Co and Cu solubility in the hydrothermal fluids (e.g., Seyfried and Ding, 1995; Metz and Trefry, 2000), indicating that most of the Co and Cu possibly precipitated in the subsurface and never reached the seafloor, which may explain the Cu-poor seafloor mineralization in these systems (**Table 2**). Alternatively, Co and Cu may not have been mobilised in significant amounts from the surrounding host rocks due to the low fluid temperatures <200°C (**Table 1**; Metz and Trefry, 2000).

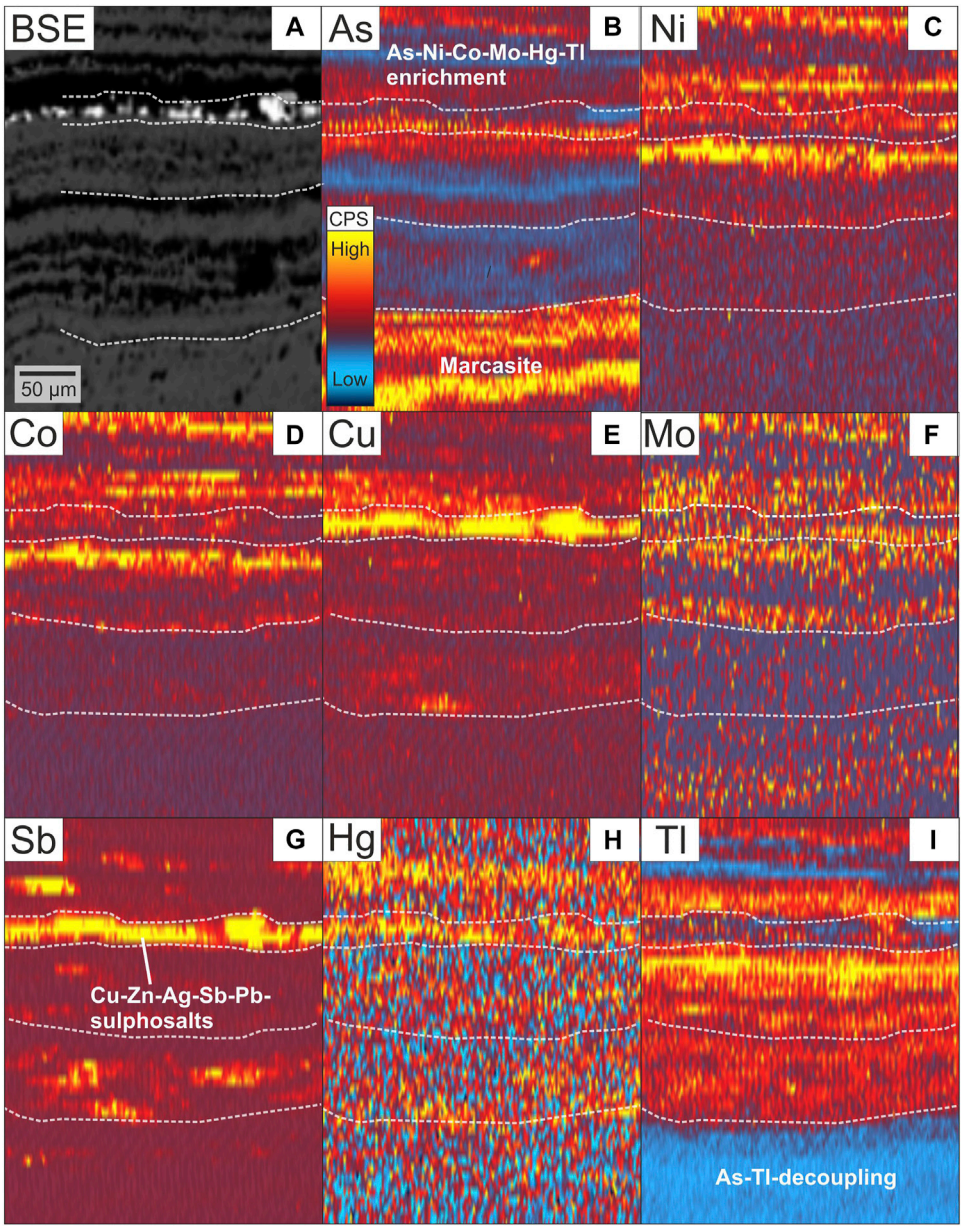

FIGURE 6 | Backscattered electron image **(A)** and trace element maps by LA-ICP-MS **(B–I)** of colloform pyrite-marcasite from Paleochori Bay. Sulphosalts hosted by amorphous silica layers (**Figure 3I**) show an enrichment of Cu, Zn, Ag, Sb and Pb. Note the coupling (As, Ni, Co, Mo, Hg, Tl) and decoupling (As, Tl) of elements between different layers in the colloform pyrite-marcasite assemblage, as highlighted by the white dashed lines.

TABLE 4 | Comparison of $\delta^{34}S$ data from this study and other shallow marine vent sites.

Sample site	Sample type	$\delta^{34}S$-value	References
Calypso SE	S Globules	−7.6 to −9.1	This study
Calypso SW	Crystalline S	0.7–3.4	This study
Calypso N	S Crust	5.7–6.7	This study
Paleochori bay	Pyrite	−4.4 to −10.8	Houghton et al. (2019)
Punta mita	Pyrite	−10.7–4.9	Alfonso et al. (2003)
Kueishantao	Native S	0.2–2.4	Yu et al. (2019)
Tyrrhenian sea	Pyrite	−32.8 to −1.1	Peters et al. (2011)

Colloform pyrite-marcasite textures are also known from deeper hydrothermal systems (>200 mbsl) in arc and back-arc environments (de Ronde, et al., 2003; Berkenbosch et al., 2012; Wohlgemuth-Ueberwasser et al., 2015; Keith et al., 2016a). However, the silicate and heavy mineral (sulphosalt) layers between colloform pyrite-marcasite at Paleochori Bay are uncommon in these deeper systems, suggesting distinct hydrodynamic precipitation conditions. Hydrothermal vent systems in very shallow water depths (<10 mbsl), such as Paleochori Bay (**Tables 1,2**), are affected by wave action, and

therefore by seasonal variations in wind and wave intensity preventing the formation of continuous Fe-sulphide layers due to constant hydrodynamic reworking (Pichler et al., 1999; Yücel et al., 2013). We propose that due to increased wave action, for example during storm events, mixing at the fluid-seawater interface is deeper in the sediment cover (>10 cm; Yücel et al., 2013) supressing the formation of sulphides at the seafloor. Instead, detrital material including heavy minerals (e.g. sulphosalts) are deposited (**Figure 3G**), which were possibly derived from the nearby onshore epithermal mineralizations on Milos island (Kilias et al., 2001; Naden et al., 2005). At decreasing wave action, the seawater-fluid interface moves upward towards the seafloor leading to the formation of colloform pyrite-marcasite upon mixing of the discharging fluid with ambient seawater (**Figure 3**).

Cinnabar (HgS) has been described at Paleochori Bay (Voudouris et al., 2021) and a similar Hg-rich mineralization has also been observed at Calypso SE (**Figure 3C**; Stoffers et al., 1999a), which is associated with charcoal fragments hosted by the volcaniclastic sediments (**Supplementary Figure S1B**). This may imply that the Hg precipitation is related to organic matter, as suggested by Prol-Ledesma et al., (2002) for the Punta Mita vent system, Mexico. Beyond this, Hg is supposed to be enriched in shallow marine hydrothermal systems due to the occurrence of boiling and its precipitation from vapor-rich fluids according to the following **equation (1)** by Varekamp and Buseck (1984).

$$Hg^{0}_{(g)} + H_2S_{(g)} \rightarrow HgS_{(S)} + H_2 \quad (1)$$

Fluid boiling has been suggested for Calypso Vents (Schwarz-Schampera et al., 2007; Hocking et al., 2010) and Paleochori Bay (Valsami-Jones et al., 2005; Wu et al., 2016), and the presence of oil, bitumen and charcoal at Calypso SE (**Supplementary Figure S1B**; Stoffers et al., 1999b; Botz et al., 2002) probably promotes the Hg mobility, and therefore leads to an oversaturation of Hg in the boiled fluids indicated by Hg droplets (Varekamp and Buseck 1984) that may subsequently be incorporated in the precipitating sulphides like pyrite (**Figure 3C**).

Coatings of Fe-sulphide around magnetite grains, as observed at Calypso Vents and Paleochori Bay (**Figures 3A,L**), are the result of magnetite sulfidation by an H_2S-rich acidic fluid in the presence of seawater oxygen according to the following **Eq. (2)** by Qian et al., (2010):

$$Fe_3O_4 + 6H_2S_{(aq)} + O_{2\,(aq)} \rightarrow 3FeS_2 + 6H_2O \quad (2)$$

This combined leaching and replacement process of detrital magnetite was also described at other shallow marine hydrothermal vents, such as Lihir, Papua New Guinea (Pichler et al., 1999) and Punta Mita, Mexico (Prol-Ledesma et al., 2002). The presence of alunite-jarosite at Paleochori Bay suggests the occurrence of oxidised low pH (<3) fluids likely reflecting a boiling-related vapor-dominated origin (Valsami-Jones et al., 2005; Price et al., 2013; Voudouris et al., 2021; Wu et al., 2016). Marcasite is only stable at low pH (<5) conditions (Murowchick and Barnes, 1986), and hence we propose that the pyrite-marcasite alternations, as observed at Paleochori Bay (**Figure 3**) may be the result of the periodic discharge of lower pH vapor-dominated fluids (cf. Pichler et al., 1999), causing the precipitation of marcasite instead of pyrite. However, acid alteration such as kaolinite or alunite is lacking at Calypso Vents (Marumo and Hattori 1999; Simmons and Brown 2000), where an alteration assemblage consisting of smectite, illite and opaline silica rather suggests neutral pH conditions (**Table 2**; Hocking et al., 2010). Hence, if an acidic alteration assemblage was present at Calypso Vents, then it was likely overprinted by a near neutral seawater-dominated fluid leading to the observed smectite-illite alteration (de Ronde et al., 2019).

Fluid Boiling and Metal Deposition

Significant variations in vent fluid chlorinity (43–2000 mM Cl) relative to seawater (~560 mM Cl) together with venting of vapor-rich fluids at Calypso Vents and Paleochori Bay indicate that boiling is a common process (Valsami-Jones et al., 2005; Schwarz-Schampera et al., 2007; Hocking et al., 2010; Price et al., 2013). Trace element partitioning typically occurs between the low-Cl vapor (e.g., As, Mo, Sb, Hg, Tl) and high-Cl liquid phase (e.g., Co, Zn, Pb; Xiong 2007; Pokrovksi et al., 2013; Brugger et al., 2016; Román et al., 2019; Keith et al., 2020), which has recently been proposed to be preserved by trace element variations (e.g. concentric zoning) in epithermal pyrite (Tardani et al., 2017; Román et al., 2019; Keith et al., 2020).

Trace element mapping of vein-type pyrite from Calypso SE reveals such concentric zoning patterns with a coupled enrichment of volatile elements like As, Mo, Sb, Hg and Tl (**Figure 5**). By contrast, concentrations of trace elements that usually form Cl-complexes in hydrothermal fluids (e.g., Co, Zn, Ag, Cd, Pb) are near or below the minimum detection limit (<0.01 ppm, **Supplementary Figure S2**), indicating that the mineralising seafloor fluids may have been vapor-dominated and of low chlorinity. This is supported by generally low Co and Pb contents in pyrite from Calypso SE (**Figure 4**), as well as a Co depletion and an Sb, Hg and Tl enrichment in vein-type compared to the fine-grained host-rock related pyrite at this vent site (**Table 3**; **Figure 4**). The distinct fractionation behaviour of As and Co between the vapor and liquid phase, respectively (Pokrovksi et al., 2013; Brugger et al., 2016; Tardani et al., 2017), suggests that the high As/Co ratios (up to 300,000) in pyrite from Calypso SE are caused by a precipitation from a vapor-rich fluid (**Figure 4B**, **8B**). By contrast, the lowest As/Co ratios in pyrite were observed at Calypso N and Paleochori Bay indicating a smaller vapor proportion in the mineralising fluids (**Figure 4B**, **Figure 8B**). Hence, the As/Co ratio in pyrite may represent a suitable tool to distinguish vapor- and liquid-dominated fluids (cf. Tardani et al., 2017; Román et al., 2019). Pyrite in the barite-cemented tuffs from Calypso SW shows high Zn, Ag and Pb contents (**Figure 4**), which suggests, together with the presence of sphalerite, argentite and galena (**Table 2**) that the corresponding hydrothermal fluids were enriched in Zn, Ag, Ba and Pb compared to the other vent sites. These elements typically concentrate in the liquid phase during vapor loss by boiling (Suzuki et al., 2008; Pokrovksi et al., 2013; Brugger et al., 2016), which may indicate a precipitation from an upwelling (high-Cl) liquid-dominated fluid with only a minor vapor proportion that formed by sub-seafloor boiling (**Figure 8B**).

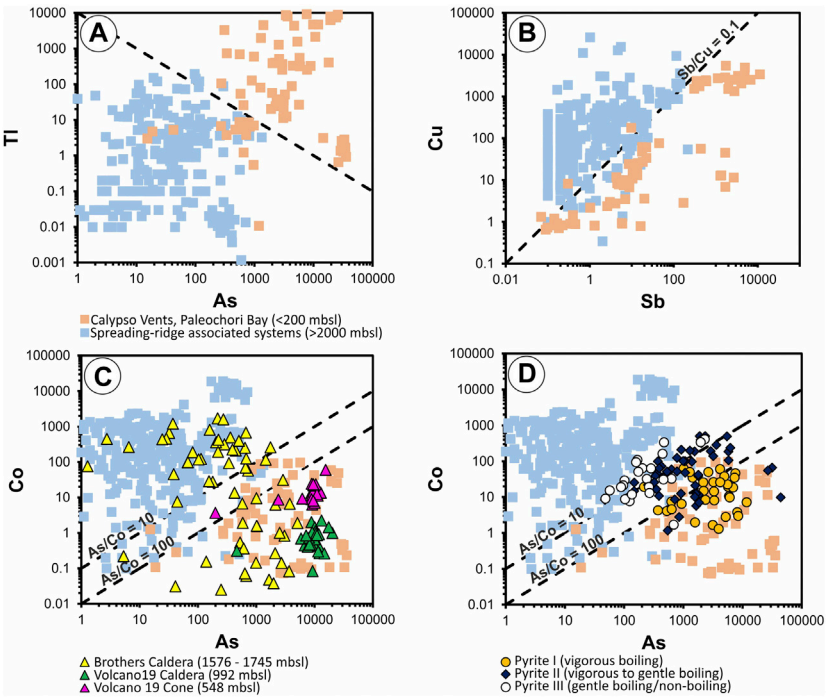

FIGURE 7 | Variation diagrams **(A–D)** comparing the trace element composition of pyrite from Calypso Vents and Paleochori Bay (<200 mbsl) with deep mid-ocean ridge-related hydrothermal sytems (>2000 mbsl). Pyrite from shallow arc-related vents (<200 mbsl) is characterised by significantly higher As, Sb, Tl and lower Cu, Co concentrations **(A–C)**, as well as higher ratios of Sb/Cu (>0.1) and As/Co (>10–100) than its deeper mid-ocean ridge-related counterparts **(C,D)**. Note that pyrite from the deeper arc-related hydrothermal systems of Brothers volcano and Volcano 19 (>200 mbsl; Keith et al., 2016a) overlaps with the mid-ocean ridge data indicating that the As/Co ratio in pyrite should not be suitable to distinguish shallower (>200 mbsl) and deeper (>200 mbsl) arc-related hydrothermal systems **(D)** Shallow arc-related pyrite (<200 mbsl) shows similar As/Co (>10–100) ratios as pyrite from boiling zones in the Cerro Pabellón Geothermal System, Chile (Román et al., 2019), indicating that fluid boiling is a key processes controlling the As/Co distribution in shallow marine hydrothermal pyrite (<200 mbsl; see text for details). Note that the dashed line in the As-Tl diagram **(A)** is not a linear function with a constant slope in linear scale, and hence it cannot statically be defined by a ratio. Pyrite data from mid-ocean ridge hydrothermal systems after: Wang et al., 2017 (~3000 m); Wang et al., 2018 (~2450 m); Grant et al., 2018 (>3500 m); Meng et al., 2020 (~2900 m).

In contrast to vein-type pyrite from Calypso SE, which is likely related to a focused fluid flow, the colloform Fe-sulphide alternations from Paleochori Bay rather formed under conditions of higher porewater/seawater influence (**Figure 8B**), and therefore do not preserve a pristine precipitation signature from a boiling hydrothermal fluid that lacks a seawater overprint (Valsami-Jones et al., 2005; Price et al., 2013). Price et al. (2013) also suggested that mixing of phase separated fluids with seawater at Paleochori Bay is a common process. Beyond this, Price et al. (2013) observed an As-Cl-rich fluid at Paleochori Bay carrying both vapor- (Sb and Tl) and liquid-related (Ag, Zn and Pb) elements, which they refer to sub-surface re-mixing of phase separated fluids. A similar process may be observed at Calypso SW and preserved by high concentrations of Sb (up to 1.1 wt%) and Tl (up to 0.9 wt%) together liquid-related elements like Zn, Ag and Pb in pyrite (**Figure 4**). In addition, crystal structures may also play an important role in the incorporation of trace elements into pyrite and marcasite (Deditius and Reich, 2016; Keith et al., 2018a). Marcasite is a polymorph of pyrite and isostructural with arsenopyrite, which leads to a higher capacity of the orthorhombic marcasite lattice to host As compared to cubic pyrite (Simon et al., 1999; Reich and Becker, 2006). This may explain the enrichment of As in the marcasite compared to the pyrite layers at Paleochori Bay (**Figure 6B**). Hence, we propose that a combination of mixing between phase separated fluids and porewater/seawater together with a crystallographic control on the trace element incorporation into pyrite and marcasite (cf. *Precipitation and Alteration Processes*) likely caused the complex trace element distribution at Paleochori Bay.

Gold contents in pyrite and marcasite from Calypso Vents and Paleochori Bay are very low (<0.6 ppm), which may be explained by the precipitation of Au in sub-seafloor boiling zones (**Figure 8B**). For example, the precipitation of Au in epithermal systems is typically related to boiling zones, where H_2S partitions into the vapor phase causing a destabilisation of the $(Au(HS)_2^-)$ complex initiating Au deposition (Drummond and Ohmoto, 1985; Cooke and McPhail 2001; Simmons et al., 2005; Keith et al., 2020). The vicinity of Calypso Vents and Paleochori Bay to Au-rich epithermal systems, such as White Island or the Taupo Volcanic zone, New Zealand (Hedenquist et al., 1993; Simmons and Brown, 2000) and Profitis Ilias or Chondro Vouno, Milos (**Figure 8A**; Naden et al., 2005; Alfieris et al., 2013), respectively, provides

evidence that the hydrothermal fluids were Au-bearing before they intersected the boiling curve during fluid ascent, indicating that most of the Au likely precipitated in the sub-seafloor environment and never reached the seafloor. We conclude that precipitation processes at shallow marine hydrothermal systems (<200 mbsl) are controlled by fluid boiling leading to the formation of phase separated vapor- and liquid-rich fluids that mix with seawater/porewater at or near the seafloor (**Figure 8B**).

Geochemical Fingerprints in Pyrite for Water Depth and Tectonic Setting

The chemical composition of vent fluids varies between island arc, back-arc and mid-ocean ridge hydrothermal systems, which is based on 1) variable contributions of magmatic volatiles, 2) leaching of magmatic host rocks from ultramafic to felsic composition and 3) differences in fluid temperature, water depth and salinity, affecting processes like phase separation (Reeves et al., 2011; Monecke et al., 2014; Kleint et al., 2015; Seewald et al., 2015; Humphris and Klein, 2017; Schmidt et al., 2017). The trace element composition of pyrite is sensitive to changes in fluid composition (Wohlgemuth-Ueberwasser et al., 2015; Keith et al., 2016a; Monecke et al., 2016; Fuchs et al., 2019; Román et al., 2019; Keith et al., 2020), and may therefore preserve a geochemical signature reflecting the tectonic and geodynamic setting of the host hydrothermal system.

Pyrite from shallow island arc-related hydrothermal vents (<200 mbsl) is characterised by a Co and Cu depletion along with an As, Sb and Tl enrichment compared to deeper spreading-related hydrothermal systems (>2000 mbsl, **Figure 7**). The higher Sb/Cu (>0.1; **Figure 7B**) and As/Co. (>100; **Figure 7C**) ratios in pyrite from shallow arc compared to deeper spreading-related hydrothermal systems (As/Co < 100; Sb/Cu < 0.1) suggest a decreasing vapor proportion in the hydrothermal fluids with increasing water depth, which may be related to stronger boiling effects and vapor-liquid separation at lower temperature-pressure conditions (Drummond and Ohmoto, 1985; Breuer and Pichler, 2013; Monecke et al., 2014; Keith et al., 2020). This is confirmed by the As/Co ratio in pyrite from the Cerro Pabellón Geothermal System, Chile (Román et al., 2019), which formed under non-boiling (As/Co<10) to vigorously boiling conditions (As/Co > 100; **Figure 7D**). Pyrite data from deeper island arc-related hydrothermal systems (>200 mbsl), such as Volcano 19 (548–992 mbsl) and Brothers volcano (1576–1745 mbsl) from the Tonga-Kermadec arc (Keith et al., 2016a), show As/Co ratios indicating boiling and non-boiling conditions. For example, pyrite from Volcano 19 exhibits As/Co ratios ranging from 1500 to 110,000 (**Figure 7C**), indicating that boiling is an important hydrothermal process, which is confirmed by fluid temperatures (245–265°C) on the seawater boiling curve, visual evidence by clear fluids with "flames" of water vapor at the seafloor, and associated sulphide dendrite formation (Stoffers et al., 2006; Keith et al., 2016a). By contrast, As/Co ratios in pyrite from the Brothers NW caldera vent system (1576–1745 mbsl) vary from 0.05 to 1100, and therefore suggest boiling (As/Co > 100) and non-boiling conditions (As/Co < 10; **Figure 7C**). Hence, we conclude that As/Tl, As/Sb and As/Co ratios in pyrite vary systematically between shallow island arc volcanoes (<200 mbsl) and deeper seafloor spreading-related hydrothermal systems (>2000 mbsl), but may not be used as a discrimination tool between shallow (<200 mbsl) and deep (>200 mbsl) island arc-related hydrothermal systems (**Figure 7C**).

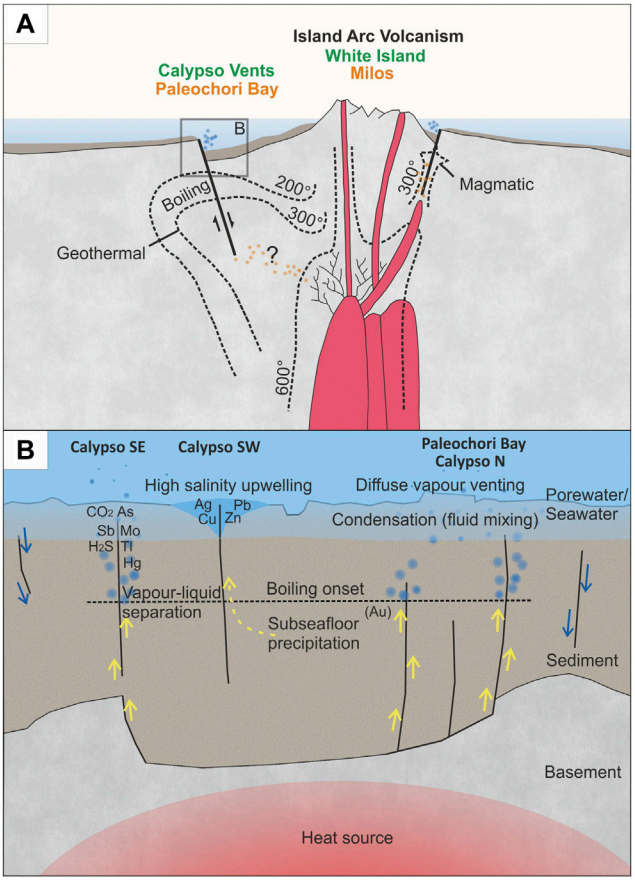

FIGURE 8 | Schematic hydrothermal model for Calypso Vents and Paleochori Bay, and their relation to nearby subaerial island arc epithermal systems, such as White Island (New Zealand) and Milos Island (Greece) **(A)** The mineralization at Calypso Vents and Paleochori Bay is mainly based on a seawater derived fluid phase, which underwent phase separation during its ascent to the seafloor. The underlying magmatic system mainly acts as a heat source that drives the seawater circulation; a direct contribution of metal- and metalloid-bearing fluids seems to be unlikely (modified after Hedenquist and Lowenstern, 1994) **(B)** Boiling in the sub-seafloor leads to the formation of vapor- and liquid-dominated fluids that either reach the seafloor, as observed at Calypso SE and SW, respectively, or mix with porewater/seawater in the volcaniclastic sediments at shallow depth, as proposed for Calypso N and Paleochori Bay. This leads to a texturally diverse and chemically distinct pyrite-marcasite paragenesis (see text for details).

Sulfur Origin and Sulfidation State

Sulfur crusts and crystalline S from Calypso N and SW, respectively, show $\delta^{34}S$ values from 0.7 to 6.7‰ (**Table 4**),

which reflect a S contribution by igneous host rock leaching ($\delta^{34}S$ ~0‰) and thermochemical seawater sulphate reduction ($\delta^{34}S$ ~21‰; Shanks, 2001; Ono et al., 2007; Keith et al., 2016b; Martin et al., 2020). In contrast, S globules from Calypso SE and hydrothermal pyrite from Paleochori Bay (Houghton et al., 2019) exhibit negative $\delta^{34}S$ values ranging from −7.6 to −9.1‰ (**Table 4**) and −4.4 to −10.8‰, respectively. These values overlap with hydrothermal pyrite hosted by volcaniclastic sediments at the Palinuro volcanic complex (Tyrrhenian Sea), which exhibit highly negative $\delta^{34}S$ values ranging from −32.8 to −1.1‰ and multiple S isotope analyses ($\delta^{34}S$ and $\Delta^{33}S$) indicate that microbial sulphate reduction caused the negative $\delta^{34}S$ signature (Peters et al., 2011; Petersen et al., 2014).

In addition to microbial sulphate reduction at lower fluid temperatures (<150°C), the disproportionation of magmatically derived SO_2 commonly also results in negative $\delta^{34}S$ values in hydrothermal precipitates (Herzig et al., 1998; Kusakabe et al., 2000; Kim et al., 2004; de Ronde et al., 2011; Martin et al., 2020). Hence, native S globules (S^0 in **Eq. (3)**) and pyrite (H_2S in Eq. (4)) with negative $\delta^{34}S$ values at Calypso SE and Paleochori Bay, respectively, could also be related to the influx of magmatic fluids followed by the hydration and disproportionation of SO_2 according to the following (**Eqs. 3,4**) by Kusakabe et al., (2000):

$$3SO_2 + 2H_2O \rightarrow 2HSO_4^- + S^0 + 2H^+ \quad (3)$$

$$4SO_2 + 4H_2O \rightarrow 3HSO_4^- + H_2S + 3H^+ \quad (4)$$

Hedenquist et al., (1993) also proposed that the disproportionation of magmatically derived SO_2 resulted in native S deposition in the active epithermal system of White Island, some 10 km north of Calypso Vents (**Figure 1B** and **Figure 8A**). Mineralogical evidence like orpiment, realgar and native S (**Table 2**) as well as the occurrence of hydrothermal fluids with pH values of ~2 at Paleochori Bay (Valsami-Jones et al., 2005) may also point towards an intermediate to high-sulfidation regime indicating a magmatic fluid contribution (Einaudi et al., 2005).

Alternatively, intermediate to high-sulfidation conditions could be due to the condensation of boiling-induced low-density vapors that are characterised by high H_2S to base metal ratios (Drummond and Ohmoto, 1985; Marumo and Hattori, 1999; Kusakabe et al., 2000). Vapor-dominated fluids in shallow low-pressure systems cannot carry large amounts of metals due to their low density (Pokrovski et al., 2013), and hence metal precipitation from these fluids leads to an excess in reduced sulfur causing native S deposition through oxygenation at the fluid-seawater/porewater interface (Kusakabe et al., 2000). This typically leads to an acidic and oxidised (SO_4^{2-} rich) alteration assemblage, which is reflected by the occurrence of alunite-jarosite at Paleochori Bay (Voudouris et al., 2021). We believe that a boiling-induced steam-heated environment is more likely at Paleochori Bay, since there are no examples for high-sulfidation epithermal systems on Milos Island. However, there is no evidence for acid alteration at Calypso Vents and the preserved alteration assemblage of smectite, illite and opaline silica is thought to rather reflect near neutral pH conditions (Hocking et al., 2010). This is consistent with a low-sulfidation environment, where magmatic fluids play a minor role (**Figure 8A**; Hedenquist and Lowenstern, 1994; Einaudi et al., 2005). If an acidic alteration assemblage was present at Calypso Vents, then it was likely overprinted by a seawater-dominated fluid leading to the observed smectite-illite alteration.

Hence, the negative $\delta^{34}S$ composition of native S and hydrothermal pyrite from Calypso SE (-7.6 to -9.1‰; **Table 4**) and Paleochori Bay (-4.4 to -10.8‰; Houghton et al., 2019) together with the observed alteration assemblage provide evidence for both SO_2 disproportionation and microbial sulphate reduction. Multiple S isotopes would allow to distinguish these two processes, which is part of future research (Peters et al., 2011; McDermott et al., 2015). However, irrespective of the S source, which cannot be fully resolved by the methods applied to this study, there is evidence that Calypso Vents and Paleochori Bay represent submarine extensions to the epithermal/geothermal systems of the Taupo Volcanic zone or White Island (New Zealand) and Milos Island (Greece), respectively (**Figure 7A**).

SUMMARY AND CONCLUSIONS

Low temperature (<200°C) island arc-related vent sites that are associated with volcaniclastic sediments at shallow water depth (<200 mbsl) are characterised by an epithermal-style mineralization that is chemically and mineralogically distinct compared to deeper arc/back arc (>200 mbsl) and mid-ocean ridge-related environments (>2000 mbsl). For example, hydrothermal pyrite and marcasite from these shallow systems (<200 mbsl) show an As, Sb and Tl enrichment and a Co and Cu depletion compared to their deeper spreading-related counterparts (>2000 mbsl). Fluid boiling, as indicated by low-Cl vapor- and high-Cl liquid-dominated fluids, is a common process in shallow marine hydrothermal systems, like Calypso Vents and Paleochori Bay, causing trace element fractionation between the vapor (e.g., As, Sb, Tl) and liquid (e.g., Co, Zn, Ag, Pb) phase. Hence, pyrite that forms from vapor-rich fluids typically shows high As/Co ratios and enrichments in As, Sb and Tl (e.g. Calypso SE) compared to pyrite that precipitates form liquid-dominated fluids (e.g. Calypso SW). Condensation of such vapor-rich fluids into seawater/porewater in a steam-heated environment results in an acidic alteration assemblage, which is preserved at Paleochori Bay (alunite-jarosite), whereas the illite-smectite alteration at Calypso Vents likely reflects an overprint by a near neutral pH fluid, possibly seawater. The $\delta^{34}S$ composition of native S varieties from Calypso Vents, together with hydrothermal pyrite from Paleochori Bay suggest that S was primarily leached from the host rocks and derived from seawater by thermochemical and microbial sulphate reduction. Clear evidence for a magmatic fluid contribution is lacking, however, without multiple S isotope data it remains enigmatic, whether the negative $\delta^{34}S$ values in native S and pyrite from Calypso SE and Paleochori Bay, respectively, are due to microbial sulphate reduction, SO_2 disproportionation or both. We propose a hydrothermal model, where fluid boiling, host rock leaching and seawater/porewater mixing together with microbial sulphate reduction and/or SO_2 disproportionation are crucial processes causing the shallow marine epithermal-style mineralization at Calypso Vents and Paleochori Bay.

DATA AVAILABILITY STATEMENT

The original contributions presented in the study are included in the article/**Supplementary Material**, further inquiries can be directed to the corresponding author.

AUTHOR CONTRIBUTIONS

MN prepared the samples for analysis and wrote the manuscript. MKe did the microprobe analyses and participated in writing and scientific discussion. KH designed the project and participated in writing and scientific discussion. RK did the LA-ICP-MS analyses and participated in writing and scientific discussion. Panagiotis Voudouris participated in microscopic work and in writing and scientific discussion. US provided geologic data on the Calypso vents area and participated in scientific discussion. HS did the S isotope analyses and participated in writing and scientific discussion. MKa provided data on the Milos hydrothermal vents and participated in writing and scientific discussion. AM provided data on the Milos hydrothermal vents and participated in writing and scientific discussion.

FUNDING

We thank the German Bundesministerium für Bildung und Forschung (BMBF) for funding of the project 03G0135A.

ACKNOWLEDGMENTS

The authors would like to thank the associate editor JH and two reviewers ZY and AM for their comments that improved the quality of the manuscript. We thank Helene Brätz and Thomas Günther for their assistance during the LA-ICP-MS and EPMA study, respectively. We acknowledge the help of Stefan Krumm during the XRD study as well as Eva Valsami-Jones for taking samples at Paleochori Bay.

SUPPLEMENTARY MATERIAL

The Supplementary Material for this article can be found online at: https://www.frontiersin.org/articles/10.3389/feart.2021.641654/full#supplementary-material.

Supplementary Figure S1. (A) Sulphur globules attached to tuff sample from Calypso SE (SO-135-110DR). (B) Thin section scan from tuff sample (SO-135-113DR7) from an area between Calypso SE and SW contains pumiceous fragments and charcoal embedded in layers of ash sediments.

Supplementary Figure S2. Qualitative trace element maps of all investigated elements from zones and inclusions in vein-type pyrite from Calypso SE (SO-135-110DR). Cobalt, Ni, Ga, Ge, Se, Cd, In and Te display concentrations below detection limit.

Supplementary Figure S3. Qualitative trace element maps of all investigated elements from colloform pyrite and marcasite alternation with Cu-Zn-Ag-Sb-Bi-In-Pb-bearing sulphosalt grains in sulphide mounds from Paleochori Bay. Gallium, Ge, Se, Cd and Te display concentrations below detection limit.

REFERENCES

Alfieris, D., Voudouris, P., and Spry, P. G. (2013). Shallow submarine epithermal Pb-Zn-Cu-Au-Ag-Te mineralization on western Milos island, aegean Volcanic Arc, Greece: mineralogical, geological and geochemical constraints. *Ore Geology. Rev.* 53, 159–180. doi:10.1016/j.oregeorev.2013.01.007

Alfonso, P., Prol-Ledesma, R. M., Canet, C., Melgarejo, J. C., and Fallick, A. E. (2003). Sulfur isotope geochemistry of the submarine hydrothermalcoastal vents of Punta Mita, Mexico. *J. Geochemical Exploration* 78–79, 301–304. doi:10.1016/S0375-6742(03)00144-4

Berkenbosch, H. A., de Ronde, C. E. J., Gemmell, J. B., McNeill, A. W., and Goemann, K. (2012). Mineralogy and formation of black smoker chimneys from Brothers submarine volcano, Kermadec arc. *Econ. Geology.* 107, 1613–1633. doi:10.2113/econgeo.107.8.1613

Binns, R. A., and Scott, S. D. (1993). Actively forming polymetallic sulfide deposits associated with felsic volcanic rocks in the eastern Manus back-arc basin, Papua New Guinea. *Econ. Geology*. 88, 2226–2236. doi:10.2113/gsecongeo.88.8.2226

Botz, R., Wehner, H., Schmitt, M., Worthington, T. J., Schmidt, M., and Stoffers, P. (2002). Thermogenic hydrocarbons from the offshore Calypso hydrothermal field, Bay of Plenty, New Zealand. *Chem. Geology.* 186, 235–248. doi:10.1016/S0009-2541(01)00418-1

Breuer, C., and Pichler, T. (2013). Arsenic in marine hydrothermal fluids. *Chem. Geology.* 348, 2–14. doi:10.1016/j.chemgeo.2012.10.044

Brugger, J., Liu, W., Etschmann, B., Mei, Y., Sherman, D. M., and Testemale, D. (2016). A review of the coordination chemistry of hydrothermal systems, or do coordination changes make ore deposits? *Chem. Geology.* 447, 219–253. doi:10.1016/j.chemgeo.2016.10.021

Canet, C., Prol-Ledesma, R. M., Proenza, J. A., Rubio-Ramos, M. A., Forrest, M. J., Torres-Vera, M. A., et al. (2005). Mn-Ba-Hg mineralization at shallow submarine hydrothermal vents in Bahía Concepción, Baja California Sur, Mexico. *Chem. Geology.* 224, 96–112. doi:10.1016/j.chemgeo.2005.07.023

Chen, C.-T. A., Zeng, Z., Kuo, F.-W., Yang, T. F., Wang, B.-J., and Tu, Y.-Y. (2005). Tide-influenced acidic hydrothermal system offshore NE Taiwan. *Chem. Geology.* 224, 69–81. doi:10.1016/j.chemgeo.2005.07.022

Cooke, D. R., and McPhail, D. C. (2001). Epithermal Au-Ag-Te mineralization, acupan, baguio district,Philippines: numerical simulations of mineral deposition. *Econ. Geology.* 96, 109–131. doi:10.2113/gsecongeo.96.1.109

Davey, F. J., Henrys, S. A., and Lodolo, E. (1995). Asymmetric rifting in a continental back-arc environment, North Island, New Zealand. *J. Volcanology Geothermal Res.* 68, 209–238. doi:10.1016/0377-0273(95)00014-L

de Ronde, C. E., Faure, K., Bray, C. J., Chappell, D. A., and Wright, I. C. (2003). Hydrothermal fluids associated with seafloor mineralization at two southern Kermadec arc volcanoes, offshore New Zealand. *Miner Deposita*. 38, 217–233. doi:10.1007/s00126-002-0305-4

de Ronde, C. E. J., Humphris, S. E., Höfig, T. W., and Reyes, A. G. (2019). IODP expedition 376 scientistsCritical role of caldera collapse in the formation of seafloor mineralization: the case of Brothers volcano. *Geology.* 47, 762–766. doi:10.1130/G46047.1

de Ronde, C. E. J., Massoth, G. J., Butterfield, D. A., Christenson, B. W., Ishibashi, J., Ditchburn, R. G., et al. (2011). Submarine hydrothermal activity and gold-rich mineralization at Brothers volcano, Kermadec arc, New Zealand. *Miner Deposita* 46, 541–584. doi:10.1007/s00126-011-0345-8

de Ronde, C. E. J., Stoffers, P., Garbe-Schönberg, D., Christenson, B. W., Jones, B., Manconi, R., et al. (2002). Discovery of active hydrothermal venting in Lake Taupo, New Zealand. *J. Volcanology Geothermal Res.* 115, 257–275. doi:10.1016/S0377-0273(01)00332-8

Deditius, A. P., and Reich, M. (2016). Constraints on the solid solubility of Hg, Tl, and Cd in arsenian pyrite. *Am. Mineral.* 101, 1451–1459. doi:10.2138/am-2016-56010.2138/am-2016-5603

Diehl, A., de Ronde, C. E. J., and Bach, W. (2020). Subcritical phase separation and occurrence of deep-seated brines at the NW Caldera vent field, Brothers volcano: evidence from fluid inclusions in hydrothermal precipitates. *Geofluids*. 2020, 1–22. doi:10.1155/2020/8868259

Drummond, S. E., and Ohmoto, H. (1985). Chemical evolution and mineral deposition in boiling hydrothermal systems. *Econ. Geology.* 80, 126–147. doi:10.2113/gsecongeo.80.1.126

Einaudi, M. T., Hedenquist, J. W., and Inan, E. E. (2005). Sulfidation state of fluids in active and extinct hydrothermal systems: transitions from porphyry to epithermal environments. *Econ. Geology.* 10, 285–313. doi:10.5382/SP.10.15

Evans, G. N., Tivey, M. K., Monteleone, B., Shimizu, N., Seewald, J. S., and Rouxel, O. J. (2020). Trace element proxies of seafloor hydrothermal fluids based on secondary ion mass spectrometry (SIMS) of black smoker chimney linings. *Geochimica et Cosmochimica Acta*. 269, 346–375. doi:10.1016/j.gca.2019.09.038

Fouquet, Y., Cambon, P., Etoubleau, J., Charlou, J. L., Ondreas, H., Barriga, F. J. A. S., et al. (2010). "Geodiversity of hydrothermal processes along the Mid-Atlantic Ridge and ultramafic-hosted mineralization: a new type of oceanic Cu-Zn-Co-Au volcanogenic massive sulfide deposit," in *Diversity of hydrothermal systems on slow spreading ocean ridges*. Editors P. Rona, J. Dyment, and B. Murton (Washington D.C.: AGU Monograph) 188, 321–368. doi:10.1029/2008GM000746

Fouquet, Y., von Stackelberg, U., Charlou, J. L., Erzinger, J., Herzig, P. M., Muehe, R., et al. (1993). Metallogenesis in back-arc environments; the Lau Basin example. *Econ. Geology.* 88, 2154–2181. doi:10.2113/gsecongeo.88.8.2154

Fuchs, S., Hannington, M. D., and Petersen, S. (2019). Divining gold in seafloor polymetallic massive sulfide systems. *Miner Deposita* 54, 789–820. doi:10.1007/s00126-019-00895-

Fytikas, M., Innocenti, F., Kolios, N., Manetti, P., Mazzuoli, R., Poli, G., et al. (1986). Volcanology and petrology of volcanic products from the island of Milos and neighbouring islets. *J. Volcanology Geothermal Res. 28*, 297-317. doi:10.1016/0377-0273(86)90028-4

Gartman, A., Hannington, M., Jamieson, J. W., Peterkin, B., Garbe-Schönberg, D., Findlay, A. J., et al. (2018). Boiling-induced formation of colloidal gold in black smoker hydrothermal fluids. *Geology* 46, 39–42. doi:10.1130/G39492.1

German, C. R., Petersen, S., and Hannington, M. D. (2016). Hydrothermal exploration of mid-ocean ridges: where might the largest sulfide deposits be forming? *Chem. Geology.* 420, 114–126. doi:10.1016/j.chemgeo.2015.11.006

Grant, H. L. J., Hannington, M. D., Petersen, S., Frische, M., and Fuchs, S. H. (2018). Constraints on the behavior of trace elements in the actively-forming TAG deposit, Mid-Atlantic Ridge, based on LA-ICP-MS analyses of pyrite. *Chem. Geology.* 498, 45–71. doi:10.1016/j.chemgeo.2018.08.019

Hannington, M. D., de Ronde, C. E. J., and Petersen, S. (2005). Sea-floor tectonics and submarine hydrothermal systems. *Econ. Geology.* 100, 111–141. doi:10.5382/AV100.06

Hannington, M., Petersen, S., and Krätschell, A. (2017). Subsea mining moves closer to shore. *Nat. Geosci* 10, 158–159. doi:10.1038/ngeo2897

Hedenquist, J. W., and Lowenstern, J. B. (1994). The role of magmas in the formation of hydrothermal ore deposits. *Nature* 370, 519–527. doi:10.1038/370519a0

Hedenquist, J. W., Simmons, S. F., Giggenbach, W. F., and Eldridge, C. S. (1993). White Island, New Zealand, volcanic-hydrothermal system represents the geochemical environment of high-sulfidation Cu and Au ore deposition. *Geology* 21, 731–734. doi:10.1130/0091-7613(1993)021%3C0731:WINZVH%3E2.3.CO;2

Herzig, P. M., Hannington, M. D., and Arribas Jr., A. (1998). Sulfur isotopic composition of hydrothermal precipitates from the Lau back-arc: implications for magmatic contributions to seafloor hydrothermal systems. *Mineralium Deposita* 33, 226–237. doi:10.1007/s001260050143

Hocking, M. W. A., Hannington, M. D., Percival, J. B., Stoffers, P., Schwarz-Schampera, U., and de Ronde, C. E. J. (2010). Clay alteration of volcaniclastic material in a submarine geothermal system, Bay of Plenty, New Zealand. *J. Volcanology Geothermal Res.* 191, 180–192. doi:10.1016/j.jvolgeores.2010.01.018

Houghton, J. L., Gilhooly, W. P., Kafantaris, F.-C. A., Druschel, G. K., Lu, G.-S., Amend, J. P., et al. (2019). Spatially and temporally variable sulfur cycling in shallow-sea hydrothermal vents, Milos, Greece. *Mar. Chem.* 208, 83–94. doi:10.1016/j.marchem.2018.11.002

Humphris, S. E., and Klein, F. (2018). Progress in deciphering the controls on the geochemistry of fluids in seafloor hydrothermal systems. *Annu. Rev. Mar. Sci.* 10, 315–343. doi:10.1146/annurev-marine-121916-063233

Jenner, F. E., O'Neill, H. S. C., Arculus, R. J., and Mavrogenes, J. A. (2010). The magnetite crisis in the evolution of arc-related magmas and the initial concentration of Au, Ag and Cu. *J. Petrology.* 51, 2445–2464. doi:10.1093/petrology/egq063

Keith, M., Haase, K. M., Klemd, R., Krumm, S., and Strauss, H. (2016b). Systematic variations of trace element and sulfur isotope compositions in pyrite with stratigraphic depth in the Skouriotissa volcanic-hosted massive sulfide deposit, Troodos ophiolite, Cyprus. *Chem. Geology.* 423, 7–18. doi:10.1016/j.chemgeo.2015.12.012

Keith, M., Haase, K. M., Klemd, R., Schwarz-Schampera, U., and Franke, H. (2017). Systematic variations in magmatic sulphide chemistry from mid-ocean ridges, back-arc basins and island arcs. *Chem. Geology.* 451, 67–77. doi:10.1016/j.chemgeo.2016.12.028

Keith, M., Haase, K. M., Klemd, R., Smith, D. J., Schwarz-Schampera, U., and Bach, W. (2018b). Constraints on the source of Cu in a submarine magmatic-hydrothermal system, Brothers volcano, Kermadec island arc. *Contrib. Mineral. Petrol.* 173, 1–16. doi:10.1007/s00410-018-1470-5

Keith, M., Haase, K. M., Schwarz-Schampera, U., Klemd, R., Petersen, S., and Bach, W. (2014). Effects of temperature, sulfur, and oxygen fugacity on the composition of sphalerite from submarine hydrothermal vents. *Geology.* 42, 699–702. doi:10.1130/G35655.1

Keith, M., Häckel, F., Haase, K. M., Schwarz-Schampera, U., and Klemd, R. (2016a). Trace element systematics of pyrite from submarine hydrothermal vents. *Ore Geology. Rev.* 72, 728–745. doi:10.1016/j.oregeorev.2015.07.012

Keith, M., Smith, D. J., Doyle, K., Holwell, D. A., Jenkin, G. R. T., Barry, T. L., et al. (2020). Pyrite chemistry: a new window into Au-Te ore-forming processes in alkaline epithermal districts, Cripple Creek, Colorado. *Geochimica et Cosmochimica Acta*. 274, 172–191. doi:10.1016/j.gca.2020.01.056

Keith, M., Smith, D. J., Jenkin, G. R. T., Holwell, D. A., and Dye, M. D. (2018a). A review of Te and Se systematics in hydrothermal pyrite from precious metal deposits: insights into ore-forming processes. *Ore Geology. Rev.* 96, 269–282. doi:10.1016/j.oregeorev.2017.07.023

Kilias, S. P., Naden, J., Cheliotis, I., Shepherd, T. J., Constandinidou, H., Crossing, J., et al. (2001). Epithermal gold mineralisation in the active aegean Volcanic Arc: the profitis Ilias deposit, Milos island, Greece. *Mineralium Deposita*. 36, 32–44. doi:10.1007/s001260050284

Kim, J., Lee, I., and Lee, K. Y. (2004). S, Sr, and Pb isotopic systematics of hydrothermal chimney precipitates from the Eastern Manus Basin, western Pacific: evaluation of magmatic contribution to hydrothermal system. *J. Geophys. Res.* 109, 1–13. doi:10.1029/2003JB002912

Kleint, C., Bach, W., Diehl, A., Fröhberg, N., Garbe-Schönberg, D., Hartmann, J. F., et al. (2019). Geochemical characterization of highly diverse hydrothermal fluids from volcanic vent systems of the Kermadec intraoceanic arc. *Chem. Geology.* 528, 119289. doi:10.1016/j.chemgeo.2019.119289

Kleint, C., Kuzmanovski, S., Powell, Z., Bühring, S. I., Sander, S. G., and Koschinsky, A. (2015). Organic Cu-complexation at the shallow marine hydrothermal vent fields off the coast of Milos (Greece), Dominica (Lesser Antilles) and the Bay of Plenty (New Zealand). *Mar. Chem.* 173, 244–252. doi:10.1016/j.marchem.2014.10.012

Kopf, A., Mascle, J., and Klaeschen, D. (2003). The Mediterranean Ridge: a mass balance across the fastest growing accretionary complex on Earth. *J. Geophys. Res.* 108, 1–22. doi:10.1029/2001JB000473

Kusakabe, M., Komoda, Y., Takano, B., and Abiko, T. (2000). Sulfur isotopic effects in the disproportionation reaction of sulfur dioxide in hydrothermal fluids: implications for the δ 34 S variations of dissolved bisulfate and elemental sulfur from active crater lakes. *J. Volcanology Geothermal Res.* 97, 287–307. doi:10.1016/S0377-0273(99)00161-4

Martin, A. J., Keith, M., McDonald, I., Haase, K. M., McFall, K. A., Klemd, R., et al. (2019). Trace element systematics and ore-forming processes in mafic VMS deposits: evidence from the Troodos ophiolite, Cyprus. *Ore Geology. Rev.* 106, 205–225. doi:10.1016/j.oregeorev.2019.01.024

Martin, A. J., Keith, M., Parvaz, D. B., McDonald, I., Boyce, A. J., McFall, K. A., et al. (2020). Effects of magmatic volatile influx in mafic VMS hydrothermal systems: evidence from the Troodos ophiolite, Cyprus. *Chem. Geology.* 531, 119325. doi:10.1016/j.chemgeo.2019.119325

Marumo, K., and Hattori, K. H. (1999). Seafloor hydrothermal clay alteration at Jade in the back-arc Okinawa Trough: mineralogy, geochemistry and isotope characteristics. *Geochimica et Cosmochimica Acta*. 63, 2785–2804. doi:10.1016/S0016-7037(99)00158-1

Maslennikov, V. V., Maslennikova, S. P., Large, R. R., Danyushevsky, L. V., Herrington, R. J., Ayupova, N. R., et al. (2017). Chimneys in Paleozoic massive sulfide mounds of the Urals VMS deposits: mineral and trace element comparison with modern black, grey, white and clear smokers. *Ore Geology. Rev.* 85, 64–106. doi:10.1016/j.oregeorev.2016.09.012

McDermott, J. M., Ono, S., Tivey, M. K., Seewald, J. S., Shanks, W. C., and Solow, A. R. (2015). Identification of sulfur sources and isotopic equilibria in submarine

hot-springs using multiple sulfur isotopes. *Geochimica et Cosmochimica Acta*. 160, 169–187. doi:10.1016/j.gca.2015.02.016

Melekestseva, I. Y., Tret'yakov, G. A., Nimis, P., Yuminov, A. M., Maslennikov, V. V., Maslennikova, S. P., et al. (2014). Barite-rich massive sulfides from the Semenov-1 hydrothermal field (Mid-Atlantic Ridge, 13°30.87′ N): evidence for phase separation and magmatic input. *Mar. Geology*. 349, 37–54. doi:10.1016/j.margeo.2013.12.013

Meng, X., Li, X., Chu, F., Zhu, J., Lei, J., Li, Z., et al. (2020). Trace element and sulfur isotope compositions for pyrite across the mineralization zones of a sulfide chimney from the East Pacific Rise (1-2°S). *Ore Geology. Rev.* 116, 103209. doi:10.1016/j.oregeorev.2019.103209

Metz, S., and Trefry, J. H. (2000). Chemical and mineralogical influences on concentrations of trace metals in hydrothermal fluids. *Geochimica et Cosmochimica Acta*. 64, 2267–2279. doi:10.1016/S0016-7037(00)00354-9

Monecke, T., Petersen, S., and Hannington, M. D. (2014). Constraints on water depth of massive sulfide formation: evidence from modern seafloor hydrothermal systems in arc-related settings. *Econ. Geology.* 109, 2079–2101. doi:10.2113/econgeo.109.8.2079

Monecke, T., Petersen, S., Hannington, M. D., and Grant, H. (2016). "The minor element endowment of modern sea-floor massive sulfide deposits and comparison with deposits hosted in ancient volcanic successions," in *Rare Earth and critical elements in Ore deposits. Reviews in economic Geology*. Editors P. L. Verplanck and M. W. Hitzman, 18, 245–306. doi:10.5382/Rev.18.11

Murowchick, J. B., and Barnes, H. L. (1986). Marcasite precipitation from hydrothermal solutions. *Geochimica et Cosmochimica Acta*. 50, 2615–2629. doi:10.1016/0016-7037(86)90214-0

Naden, J., Kilias, S. P., and Darbyshire, D. P. F. (2005). Active geothermal systems with entrained seawater as modern analogs for transitional volcanic-hosted massive sulfide and continental magmato-hydrothermal mineralization: the example of Milos Island, Greece. *Geology*. 33, 541–544. doi:10.1130/G21307.1

Nozaki, T., Ishibashi, J.-I., Shimada, K., Nagase, T., Takaya, Y., Kato, Y., et al. (2016). Rapid growth of mineral deposits at artificial seafloor hydrothermal vents. *Sci. Rep.* 6, 1–10. doi:10.1038/srep22163

Ono, S., Shanks, W. C., Rouxel, O. J., and Rumble, D. (2007). S-33 constraints on the seawater sulfate contribution in modern seafloor hydrothermal vent sulfides. *Geochimica et Cosmochimica Acta*. 71, 1170–1182. doi:10.1016/j.gca.2006.11.017

Patten, C. G. C., Pitcairn, I. K., Alt, J. C., Zack, T., Lahaye, Y., Teagle, D. A. H., et al. (2019). Metal fluxes during magmatic degassing in the oceanic crust: sulfide mineralisation at ODP site 786B, Izu-Bonin forearc. *Miner Deposita*. 55, 469–489. doi:10.1007/s00126-019-00900-9

Patten, C. G. C., Pitcairn, I. K., and Teagle, D. A. H. (2017). Hydrothermal mobilisation of Au and other metals in supra-subduction oceanic crust: insights from the Troodos ophiolite. *Ore Geology. Rev.* 86, 487–508. doi:10.1016/j.oregeorev.2017.02.019

Peters, M., Strauss, H., Petersen, S., Kummer, N.-A., and Thomazo, C. (2011). Hydrothermalism in the Tyrrhenian Sea: inorganic and microbial sulfur cycling as revealed by geochemical and multiple sulfur isotope data. *Chem. Geology.* 280, 217–231. doi:10.1016/j.chemgeo.2010.11.011

Petersen, S., Monecke, T., Westhues, A., Hannington, M. D., Gemmell, J. B., Sharpe, R., et al. (2014). Drilling shallow-water massive sulfides at the Palinuro volcanic complex, aeolian island arc, Italy. *Econ. Geology.* 109, 2129–2158. doi:10.2113/econgeo.109.8.2129

Pichler, T., Giggenbach, W. F., McInnes, B. I. A., Buhl, D., and Duck, B. (1999). Fe sulfide formation due to seawater-gas-sediment interaction in a shallow-water hydrothermal system at Lihir Island, Papua New Guinea. *Econ. Geology.* 94, 281–288. doi:10.2113/gsecongeo.94.2.281

Pokrovski, G. S., Borisova, A. Y., and Bychkov, A. Y. (2013). Speciation and transport of metals and metalloids in geological vapors. *Rev. Mineralogy Geochem.* 76, 165–218. doi:10.2138/rmg.2013.76.6

Price, R. E., Savov, I., Planer-Friedrich, B., Bühring, S. I., Amend, J., and Pichler, T. (2013). Processes influencing extreme as enrichment in shallow-sea hydrothermal fluids of Milos Island, Greece. *Chem. Geology.* 348, 15–26. doi:10.1016/j.chemgeo.2012.06.007

Prol-Ledesma, R. M., Canet, C., Melgarejo, J. C., Tolson, G., Rubio-Ramos, M. A., Cruz-Ocampo, J. C., et al. (2002). Cinnabar deposition in submarine coastal hydrothermal vents, pacific margin of central Mexico. *Econ. Geology.* 97, 1331–1340. doi:10.2113/gsecongeo.97.6.1331

Qian, G., Brugger, J., Skinner, W. M., Chen, G., and Pring, A. (2010). An experimental study of the mechanism of the replacement of magnetite by pyrite up to 300°C. *Geochimica et Cosmochimica Acta*. 74, 5610–5630. doi:10.1016/j.gca.2010.06.035

Reeves, E. P., Seewald, J. S., Saccocia, P., Bach, W., Craddock, P. R., Shanks, W. C., et al. (2011). Geochemistry of hydrothermal fluids from the PACMANUS, northeast pual and Vienna woods hydrothermal fields, manus basin, Papua New Guinea. *Geochimica et Cosmochimica Acta*. 75, 1088–1123. doi:10.1016/j.gca.2010.11.008

Reich, M., and Becker, U. (2006). First-principles calculations of the thermodynamic mixing properties of arsenic incorporation into pyrite and marcasite. *Chem. Geology.* 225, 278–290. doi:10.1016/j.chemgeo.2005.08.021

Reimann, C., and Filzmoser, P. (2000). Normal and lognormal data distribution in geochemistry: death of a myth. Consequences for the statistical treatment of geochemical and environmental data. *Environ. Geology.* 39, 1001–1014. doi:10.1007/s002549900081

Revan, M. K., Genç, Y., Maslennikov, V. V., Maslennikova, S. P., Large, R. R., and Danyushevsky, L. V. (2014). Mineralogy and trace-element geochemistry of sulfide minerals in hydrothermal chimneys from the Upper-Cretaceous VMS deposits of the eastern Pontide orogenic belt (NE Turkey). *Ore Geology. Rev.* 63, 129–149. doi:10.1016/j.oregeorev.2014.05.006

Román, N., Reich, M., Leisen, M., Morata, D., Barra, F., and Deditius, A. P. (2019). Geochemical and micro-textural fingerprints of boiling in pyrite. *Geochimica et Cosmochimica Acta*. 246, 60–85. doi:10.1016/j.gca.2018.11.034

Schmidt, K., Garbe-Schönberg, D., Hannington, M. D., Anderson, M. O., Bühring, B., Haase, K., et al. (2017). Boiling vapour-type fluids from the Nifonea vent field (New Hebrides Back-Arc, Vanuatu, SW Pacific): geochemistry of an early-stage, post-eruptive hydrothermal system. *Geochimica et Cosmochimica Acta*. 207, 185–209. doi:10.1016/j.gca.2017.03.016

Schwarz-Schampera, U., Botz, R., Hannington, M., Adamson, R., Anger, V., Cormany, D., et al. (2009). Cruise Report SONNE 192/2 (MANGO): marine geoscientific research on input and output in the Tonga-Kermadec subduction zone. *Kiel: Technische Informationsbibliothek u. Universitätsbibliothek*, 92.

Scott, R. B., Rona, P. A., McGregor, B. A., and Scott, M. R. (1974). The TAG hydrothermal field. *Nature*. 251, 301–302. doi:10.1038/251301a0

Seewald, J. S., Reeves, E. P., Bach, W., Saccocia, P. J., Craddock, P. R., Shanks, W. C., et al. (2015). Submarine venting of magmatic volatiles in the eastern manus basin, Papua New Guinea. *Geochimica et Cosmochimica Acta*. 163, 178–199. doi:10.1016/j.gca.2015.04.023

Seewald, J. S., Reeves, E. P., Bach, W., Saccocia, P. J., Craddock, P. R., Walsh, E., et al. (2019). Geochemistry of hot-springs at the SuSu Knolls hydrothermal field, Eastern Manus Basin: advanced argillic alteration and vent fluid acidity. *Geochimica et Cosmochimica Acta*. 255, 25–48. doi:10.1016/j.gca.2019.03.034

Seward, T. M., Williams-Jones, A. E., and Migdisov, A. A. (2014). "The chemistry of metal transport and deposition by ore-forming hydrothermal fluids,". *Treatise on Geochemistry*. Editors H. D. Holland and K. K. Turekian. 2nd Edition (Netherlands: Elsevier), Vol. 13, 29–57. doi:10.1016/B978-0-08-095975-7.01102-5

Seyfried, W. E., and Ding, K. (1995). "Phase equilibria in subseafloor hydrothermal systems: a review of the role of redox, temperature, pH and dissolved Cl on the Chemistry of hot spring fluids at mid-ocean ridges," in *Seafloor hydrothermal systems, physical, chemical, biological, and geological interactions.* Editors S. R. Humphris, R. A. Zierenberg, L. S. Mullineaux, and R. E. Thomson (Washington D.C.: Geophysical Monograph Series), 91, 248–272. doi:10.1029/GM091p0248

Shanks, W. C. (2001). Stable isotopes in seafloor hydrothermal systems: vent fluids, hydrothermal deposits, hydrothermal alteration, and microbial processes. *Rev. Mineralogy Geochem.* 43, 469–525. doi:10.2138/gsrmg.43.1.469

Simmons, S. F., and Brown, P. R. L. (2000). Hydrothermal minerals and precious metals in the Broadlands-Ohaaki geothermal system: implications for understanding low-sulfidation epithermal environments. *Econ. Geology.* 95, 971–999. doi:10.2113/gsecongeo.95.5.97110.2113/95.5.971

Simmons, S. F., White, N. C., and John, D. A. (2005). Geological characteristics of epithermal precious and base metal deposits. *Econ. Geology.* 100, 485–522. doi:10.5382/AV100.16

Simon, G., Huang, H., Penner-Hahn, J. E., Kesler, S. E., and Kao, L.-S. (1999). Oxidation state of gold and arsenic in gold-bearing arsenian pyrite. *Am. Mineral.* 84, 1071–1079. doi:10.2138/am-1999-7-809

Smith, D. J., Naden, J., Miles, A.-J., Bennett, H., and Bicknell, S. H. (2018). Mass wasting events and their impact on the formation and preservation of submarine ore deposits. *Ore Geology. Rev.* 97, 143–151. doi:10.1016/j.oregeorev.2018.05.008

Stoffers, P., Hannington, M., Wright, I., Herzig, P., and de Ronde, C. (1999a). Elemental mercury at submarine hydrothermal vents in the Bay of Plenty, Taupo volcanic zone, New Zealand. *Geology* 27, 931–934. doi:10.1130/0091-7613(1999)027%3C0931:EMASHV%3E2.3.CO;2

Stoffers, P., Worthington, T. J., Schwarz-Schampera, U., Hannington, M. D., Massoth, G. J., Hekinian, R., et al. (2006). Submarine volcanoes and high-temperature hydrothermal venting on the Tonga arc, southwest Pacific. *Geology*. 34, 453–456. doi:10.1130/G22227.1

Stoffers, P., and Wright, I. (1999b). Cruise Report SO 135: Havre Trough – Taupo Volcanic Zone: Tectonic, magmatic and hydrothermal processes. Kiel: Institut für Geowissenschaften, Christian-Albrecht-Universität, 250.

Stucker, V. K., Walker, S. L., de Ronde, C. E. J., Caratori Tontini, F., and Tsuchida, S. (2017). Hydrothermal venting at hinepuia submarine volcano, Kermadec arc: understanding magmatic-hydrothermal fluid chemistry. *Geochem. Geophys. Geosyst.* 18, 3646–3661. doi:10.1002/2016GC006713

Suzuki, R., Ishibashi, J.-I., Nakaseama, M., Konno, U., Tsunogai, U., Gena, K., et al. (2008). Diverse range of mineralization induced by phase separation of hydrothermal fluid: case study of the Yonaguni Knoll IV hydrothermal field in the Okinawa Trough back-arc basin. *Resource Geology*. 58, 267–288. doi:10.1111/j.1751-3928.2008.00061.x

Tardani, D., Reich, M., Deditius, A. P., Chryssoulis, S., Sánchez-Alfaro, P., Wrage, J., et al. (2017). Copper-arsenic decoupling in an active geothermal system: a link between pyrite and fluid composition. *Geochimica et Cosmochimica Acta*. 204, 179–204. doi:10.1016/j.gca.2017.01.044

Tivey, M. (2007). Generation of seafloor hydrothermal vent fluids and associated mineral deposits. *Oceanog.* 20, 50–65. doi:10.5670/oceanog.2007.80

Valsami-Jones, E., Baltatzis, E., Bailey, E. H., Boyce, A. J., Alexander, J. L., Magganas, A., et al. (2005). The geochemistry of fluids from an active shallow submarine hydrothermal system: Milos island, Hellenic Volcanic Arc. *J. Volcanology Geothermal Res.* 148, 130–151. doi:10.1016/j.jvolgeores.2005.03.018

van Achterbergh, E., Ryan, C. G., and Griffin, W. L. (2000). GLITTER: On-line interactive data reduction for the laserablation ICP-MS microprobe. *Ninth Annual V. M. Goldschmidt Conference*, August 22-27, Cambridge, Massachusetts.

Varekamp, J. C., and Buseck, P. R. (1984). The speciation of mercury in hydrothermal systems, with applications to ore deposition. *Geochimica et Cosmochimica Acta* 48, 177–185. doi:10.1016/0016-7037(84)90359-4

Varnavas, S. P., and Cronan, D. S. (2005). Submarine hydrothermal activity off Santorini and Milos in the central hellenic volcanic arc: a synthesis. *Chem. Geology*. 224, 40–54. doi:10.1016/j.chemgeo.2005.07.013

Von Damm, K. L. (1995). "Controls on the chemistry and temporal variability of fluids,". *Seafloor hydrothermal systems, physical, chemical, biological, and geological interactions*. Editors S. R. Humphris, R. A. Zierenberg, L. S. Mullineaux, and R. E. Thomson (Washington D.C: Geophysical Monograph Series), 91, 222–247. doi:10.1029/GM091p0222

Voudouris, P., Kati, M., Magganas, A., Keith, M., Valsami-Jones, E., Haase, K., et al. (2021). Arsenian pyrite and cinnabar from active submarine nearshore vents, Paleochori Bay, Milos Island, Greece. *Minerals* 11, 14–25. doi:10.3390/min11010014

Voudouris, P., Mavrogonatos, C., Spry, P. G., Baker, T., Melfos, V., Klemd, R., et al. (2019). Porphyry and epithermal deposits in Greece: an overview, new discoveries, and mineralogical constraints on their genesis. *Ore Geology. Rev.* 107, 654–691. doi:10.1016/j.oregeorev.2019.03.019

Wang, Y., Han, X., Petersen, S., Frische, M., Qiu, Z., Cai, Y., et al. (2018). Trace metal distribution in sulfide minerals from ultramafic-hosted hydrothermal systems: examples from the kairei vent field, central Indian ridge. *Minerals*. 8, 526–621. doi:10.3390/min8110526

Wang, Y., Han, X., Petersen, S., Frische, M., Qiu, Z., Li, H., et al. (2017). Mineralogy and trace element geochemistry of sulfide minerals from the wocan hydrothermal field on the slow-spreading carlsberg ridge, Indian Ocean. *Ore Geology. Rev.* 84, 1–19. doi:10.1016/j.oregeorev.2016.12.020

Wilson, C. J. N., Houghton, B. F., McWilliams, M. O., Lanphere, M. A., Weaver, S. D., and Briggs, R. M. (1995). Volcanic and structural evolution of Taupo volcanic zone, New Zealand: a review. *J. Volcanology Geothermal Res.* 68, 1–28. doi:10.1016/0377-0273(95)00006-G

Wohlgemuth-Ueberwasser, C. C., Viljoen, F., Petersen, S., and Vorster, C. (2015). Distribution and solubility limits of trace elements in hydrothermal black smoker sulfides: an *in-situ* LA-ICP-MS study. *Geochimica et Cosmochimica Acta*. 159, 16–41. doi:10.1016/j.gca.2015.03.020

Wright, I. C. (1990). Late quaternary faulting of the offshore Whakatane graben, Taupo volcanic zone, New Zealand. *New Zealand J. Geology. Geophys.* 33, 245–256. doi:10.1080/00288306.1990.10425682

Wu, Z., Sun, X., Xu, H., Konishi, H., Wang, Y., Wang, C., et al. (2016). Occurrences and distribution of "invisible" precious metals in sulfide deposits from the Edmond hydrothermal field, Central Indian Ridge. *Ore Geology. Rev.* 79, 105–132. doi:10.1016/j.oregeorev.2016.05.006

Xiong, Y. (2007). Hydrothermal thallium mineralization up to 300 °C: a thermodynamic approach. *Ore Geology. Rev.* 32, 291–313. doi:10.1016/j.oregeorev.2006.10.003

Yang, K., and Scott, S. D. (1996). Possible contribution of a metal-rich magmatic fluid to a sea-floor hydrothermal system. *Nature* 383, 420–423. doi:10.1038/383420a0

Yeats, C. J., Parr, J. M., Binns, R. A., Gemmell, J. B., and Scott, S. D. (2014). The SuSu knolls hydrothermal field, eastern manus basin, Papua New Guinea: an active submarine high-sulfidation copper-gold system. *Econ. Geology.* 109, 2207–2226. doi:10.2113/econgeo.109.8.2207

Yu, M.-Z., Chen, X.-G., Garbe-Schönberg, D., Ye, Y., and Chen, C.-T. A. (2019). Volatile chalcophile elements in native sulfur from a submarine hydrothermal system at Kueishantao, offshore NE Taiwan. *Minerals* 9, 245–318. doi:10.3390/min9040245

Yücel, M., Sievert, S. M., Vetriani, C., Foustoukos, D. I., Giovannelli, D., and Le Bris, N. (2013). Eco-geochemical dynamics of a shallow-water hydrothermal vent system at Milos Island, Aegean Sea (Eastern Mediterranean). *Chem. Geology.* 356, 11–20. doi:10.1016/j.chemgeo.2013.07.020

Conflict of Interest: The authors declare that the research was conducted in the absence of any commercial or financial relationships that could be construed as a potential conflict of interest.

The reviewer (AM) declared a past collaboration with one of the authors (MK) to the handling editor.